

Bounds-Preserving Lax-Wendroff Discontinuous Galerkin Schemes for Quadrature-Based Moment-Closure Approximations of Kinetic Models

Erica R. Johnson · James A. Rossmannith^{*} · Christine Vaughan

Received: date / Accepted: date

Abstract The quadrature-based method of moments (QMOM) offers a promising class of approximation techniques for reducing kinetic equations to fluid equations that are valid beyond thermodynamic equilibrium. A major challenge with these and other closures is that whenever the flux function must be evaluated (e.g., in a numerical update), a moment-inversion problem must be solved that computes the flux from the known input moments. In this work we study a particular five-moment variant of QMOM known as HyQMOM and establish that this system is moment-invertible over a convex region in solution space. We then develop a high-order Lax-Wendroff discontinuous Galerkin scheme for solving the resulting fluid system. The scheme is based on a predictor-corrector approach, where the prediction step is a localized space-time discontinuous Galerkin scheme. The nonlinear algebraic system that arises in this prediction step is solved using a Picard iteration. The correction step is a straightforward explicit update using the predicted solution in order to evaluate space-time flux integrals. In the absence of additional limiters, the proposed high-order scheme does not in general guarantee that the numerical solution remains in the convex set over which HyQMOM is moment-invertible. To overcome this challenge,

^{*} Corresponding author

This research was partially funded by NSF Grants DMS-1620128 and DMS-2012699.

Erica R. Johnson
Southwest Research Institute, Space Science Department,
6220 Culebra Road, San Antonio, Texas 78238, USA
E-mail: erica.johnson@swri.edu

James A. Rossmannith
Iowa State University, Department of Mathematics,
411 Morrill Road, Ames, Iowa 50011, USA
E-mail: rossmani@iastate.edu

Christine Vaughan
Iowa State University, Department of Mathematics,
411 Morrill Road, Ames, Iowa 50011, USA
E-mail: cwiersma@iastate.edu

we introduce novel limiters that rigorously guarantee that the computed solution does not leave the convex set over which moment-invertible and hyperbolicity of the fluid system is guaranteed. We develop positivity-preserving limiters in both the prediction and correction steps, as well as an oscillation-limiter that damps unphysical oscillations near shocks and rarefactions. Finally, we perform convergence tests to verify the order of accuracy of the scheme, as well as test the scheme on Riemann data to demonstrate the shock-capturing and robustness of the method.

Keywords discontinuous Galerkin · hyperbolic conservation laws · moment closure · positivity-preserving limiters

Mathematics Subject Classification (2010) 65M60 · 82C80

1 Introduction

Kinetic Boltzmann equations model the non-equilibrium dynamics of a wide variety of fluids, including gases, multiphase flows, and plasma. These equations have the following general form:

$$f_t + \underline{v} \cdot \underline{\nabla}_{\underline{x}} f + \underline{\mathcal{F}} \cdot \underline{\nabla}_{\underline{v}} f = \mathbb{C}(f), \quad (1.1)$$

where $f(t, \underline{x}, \underline{v}) : \mathbb{R}_{\geq 0} \times \mathbb{R}^D \times \mathbb{R}^V \mapsto \mathbb{R}_{\geq 0}$ is the distribution function that describes the state of the fluid, $t \in \mathbb{R}_{\geq 0}$ is time, $\underline{x} \in \mathbb{R}^D$ is the spatial coordinate, and $\underline{v} \in \mathbb{R}^V$ is the velocity coordinate. Additionally, $\underline{\mathcal{F}}(t, \underline{x}, \underline{v}) \in \mathbb{R}_{\geq 0} \times \mathbb{R}^D \times \mathbb{R}^V \mapsto \mathbb{R}^V$ is the forcing term that could include lift, drag, gravity, and other forces acting on the particles, and $\mathbb{C}(f) : \mathbb{R}_{\geq 0} \mapsto \mathbb{R}$ is the collision term that describes direct particle-particle interactions.

Kinetic models of the form (1.1) offer two desirable features: (1) the evolution equations have a relatively simple form (i.e., advection in phase space) and (2) the models are capable of accurately describing a large class of physical phenomena that are important in application problems. However, the main difficulty with kinetic models is that their solutions live in a high-dimensional phase space, which means that high fidelity numerical computations are very expensive.

One approach for reducing the computational complexity of kinetic models is to replace them with so-called *fluid models*, which means that instead of evolving the distribution function directly, one evolves a finite set of *moments* of the distribution function. Throughout this work we will be focused on the one-dimensional version of (1.1) (i.e., $D = 1$ and $V = 1$). Furthermore, since the reduction to fluid models can be done independently of the type of forcing and collision operator, we will focus here on the 1D1V Boltzmann equation in the zero-forcing ($\underline{\mathcal{F}} \equiv 0$) and collisionless ($\mathbb{C}(f) \equiv 0$) regime:

$$f_t + v f_x = 0, \quad (1.2)$$

where now $f(t, x, v) : \mathbb{R}_{\geq 0} \times \mathbb{R} \times \mathbb{R} \mapsto \mathbb{R}_{\geq 0}$ is the probability distribution function. The moments of f are defined as follows:

$$M_\ell := \int_{\mathbb{R}} v^\ell f dv, \quad \text{for } \ell \in \mathbb{N}_0. \quad (1.3)$$

A simple calculation reveals that for each $\ell \in \mathbb{N}_0$, the moments satisfy the following equation:

$$M_{\ell,t} + M_{\ell+1,x} = 0. \quad (1.4)$$

The key difficulty is that the evolution of the ℓ^{th} moment depends on the $(\ell + 1)^{\text{st}}$ moment, meaning that the moment expansion does not produce a closed system. Therefore, the key challenge for developing fluid approximations to kinetic models is then the following question: How does one close the moment hierarchy?

Definition 1.1 (Univariate moment-closure problem) Let $S \in \mathbb{N}_0$. Given only the first $S + 1$ moments of a univariate distribution function $f(v)$:

$$M_\ell = \int_{-\infty}^{\infty} v^\ell f(v) dv, \quad \text{for } \ell = 0, 1, \dots, S, \quad (1.5)$$

find an approximation of the next moment, M_{S+1} , in terms of the given moments.

The basic strategy in most moment-closure approaches is as follows: (1) start with a finite set of moments (e.g., $\ell = 0, 1, \dots, S$); (2) assume a form of the distribution function with several free parameters (typically, the number of free parameters is the same as the number of moments that will be tracked); (3) determine the free parameters in the assumed distribution function so that its moments match all of the known moments (this part is called *moment-inversion*); and (4) compute the next moment of the assumed distribution function, which is then used to provide the flux in the evolution equation for M_S :

$$M_{S,t} + \bar{M}_{S+1,x} = 0, \quad (1.6)$$

where $\bar{M}_{S+1} = \bar{M}_{S+1}(M_0, M_1, \dots, M_S)$.

1.1 Existence: Moment-Realizability

Before considering specific strategies for approximating the missing moment, M_{S+1} , it is worthwhile to discuss the general existence problem first. We begin by defining some important quantities relevant throughout this work, namely the mass density, macroscopic velocity, pressure, heat flux, and modified kurtosis:

$$\begin{aligned} \rho &:= \int_{-\infty}^{\infty} f dv, & u &:= \frac{1}{\rho} \int_{-\infty}^{\infty} v f dv, & p &:= \int_{-\infty}^{\infty} (v - u)^2 f dv, \\ q &:= \int_{-\infty}^{\infty} (v - u)^3 f dv, & \text{and} & & k &:= \int_{-\infty}^{\infty} (v - u)^4 f dv - \left(\frac{p^3 + \rho q^2}{\rho p} \right), \end{aligned} \quad (1.7)$$

where we assume that $\rho, p > 0$. These *primitive variables* are directly linked to the moments M_ℓ :

$$\begin{aligned} \rho &= M_0, & u &= \frac{M_1}{M_0}, & p &= M_2 - \frac{M_1^2}{M_0}, & q &= M_3 - \frac{3M_1M_2}{M_0} + \frac{2M_1^3}{M_0^2}, \\ \text{and} & & k &= \frac{M_2^3 - 2M_1M_2M_3 + M_0M_3^2 + M_1^2M_4 - M_0M_2M_4}{M_1^2 - M_0M_2}. \end{aligned} \quad (1.8)$$

Using these we define the *normalized velocity variable*, s , and the *normalized moments*: \tilde{M}_k :

$$s := \frac{v-u}{\sqrt{T}} \quad \text{and} \quad \tilde{M}_k := \frac{\sqrt{T}}{\rho} \int_{-\infty}^{\infty} s^k f(v(s)) ds = \int_{-\infty}^{\infty} s^k \tilde{f}(s) ds, \quad (1.9)$$

where $T = p/\rho$ is the temperature. The moments and the normalized moments are related as follows:

$$M_\ell = \rho \sum_{k=0}^{\ell} \binom{\ell}{k} T^{\frac{k}{2}} u^{\ell-k} \tilde{M}_k \quad \text{and} \quad \tilde{M}_k = \rho^{-1} T^{-\frac{k}{2}} \sum_{\ell=0}^k \binom{k}{\ell} (-u)^{k-\ell} M_\ell. \quad (1.10)$$

By construction, the normalized moments have the following property:

$$\tilde{M}_0 = 1, \quad \tilde{M}_1 = 0, \quad \text{and} \quad \tilde{M}_2 = 1. \quad (1.11)$$

Definition 1.2 (Realizable moments) *The following rescaled moments:*

$$\tilde{M}_0 = 1, \quad \tilde{M}_1 = 0, \quad \tilde{M}_2 = 1, \quad \tilde{M}_3, \quad \dots, \quad \tilde{M}_S,$$

where $S \in \mathbb{Z}_{\geq 3}$ and $|\tilde{M}_k| < \infty \forall k \in \mathbb{Z}_{\geq 0}$, are called **realizable** if there exists a probability density function, $f(s) : \mathbb{R} \mapsto \mathbb{R}_{\geq 0}$, such that

$$\tilde{M}_k = \int_{-\infty}^{\infty} s^k \tilde{f}(s) ds \quad \text{for } k = 0, 1, \dots, S.$$

This leads to an obvious question: for a given $S \in \mathbb{Z}_{\geq 3}$, under what conditions is the set of moments, $\{\tilde{M}_0 = 1, \tilde{M}_1 = 0, \tilde{M}_2 = 1, \tilde{M}_3, \dots, \tilde{M}_S\}$, realizable? This question is the celebrated **truncated Hamburger moment problem** (e.g., see Chapter 9 of [38]) for which we can state the following result. Note that we state only the case where S is even, although a similar result also exists when S is odd [38].

Theorem 1.1 (Truncated Hamburger moment problem (adapted from Theorem 9.27 of [38])) *Let $S \in \mathbb{Z}_{>3}$ be an even integer. The set of moments:*

$$\{\tilde{M}_0 = 1, \tilde{M}_1 = 0, \tilde{M}_2 = 1, \tilde{M}_3, \dots, \tilde{M}_S\}$$

is realizable if all of the Hankel determinants for $m = 0, 1, \dots, S/2$ are positive:

$$D_m := \begin{vmatrix} 1 & 0 & 1 & \tilde{M}_3 & \cdots & \tilde{M}_m \\ 0 & 1 & \tilde{M}_3 & \tilde{M}_4 & \cdots & \tilde{M}_{m+1} \\ 1 & \tilde{M}_3 & \tilde{M}_4 & \tilde{M}_5 & \cdots & \tilde{M}_{m+2} \\ \tilde{M}_3 & \tilde{M}_4 & \tilde{M}_5 & \tilde{M}_6 & \cdots & \tilde{M}_{m+3} \\ \vdots & \vdots & \vdots & \vdots & \ddots & \vdots \\ \tilde{M}_m & \tilde{M}_{m+1} & \tilde{M}_{m+2} & \tilde{M}_{m+3} & \cdots & \tilde{M}_{2m} \end{vmatrix} > 0.$$

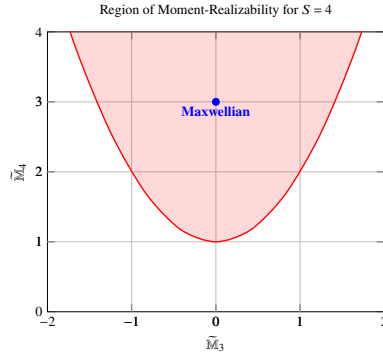


Fig. 1.1 Region of the moment-realizability when $S = 4$. In other words, given the five rescaled moments: $\tilde{M}_0 = 1$, $\tilde{M}_1 = 0$, $\tilde{M}_2 = 1$, \tilde{M}_3 , and \tilde{M}_4 , there exists a positive distribution function matching the given moments provided that these moments lie within the shaded pink region of the above graph. Thermodynamic equilibrium (i.e., the Maxwellian distribution) occurs at $\tilde{M}_3 = 0$ and $\tilde{M}_4 = 3$, which is in the interior of the shaded pink region.

1.2 Example: $S = 4$ case

As an example, which will become relevant later in this work, consider the case $S = 4$, where the three relevant Hankel determinants are

$$D_0 = 1, \quad D_1 = 1, \quad D_2 = \begin{vmatrix} 1 & 0 & 1 \\ 0 & 1 & \tilde{M}_3 \\ 1 & \tilde{M}_3 & \tilde{M}_4 \end{vmatrix} = \tilde{M}_4 - \tilde{M}_3^2 - 1 > 0. \quad (1.12)$$

Thus, the realizability condition in the univariate $S = 4$ case is

$$\tilde{M}_4 > \tilde{M}_3^2 + 1, \quad (1.13)$$

which is depicted in Figure 1.1. Also shown in this figure is the location of the distribution in thermodynamic equilibrium (i.e., the Maxwellian distribution):

$$f(v) = \frac{\rho}{\sqrt{2\pi T}} e^{-\frac{(v-u)^2}{2T}} \implies \tilde{f}(s) = \frac{1}{\sqrt{2\pi}} e^{-\frac{s^2}{2}} \implies \begin{cases} \tilde{M}_3 = 0 \\ \tilde{M}_4 = 3 \end{cases}. \quad (1.14)$$

Finally, we note that the realizability condition (1.13) in terms of the primitive variables can be written as follows:

$$\frac{\rho k}{p^2} > 0, \quad (1.15)$$

which is satisfied if $\rho > 0$, $p > 0$, and $k > 0$.

1.3 Techniques for Moment-Closure

There are many different moment closure methods that approximate the final moment \tilde{M}_{S+1} , and each method has its own merits and challenges. Three broad classes of commonly used moment-closures are briefly described below.

Grad closure: This approach was originally developed by Grad [19] in 1949, but variants with improved hyperbolicity properties have been introduced more recently [5, 6, 24]. The basic idea is that the distribution function is approximated as a Maxwellian times a polynomial:

$$\tilde{f}(s) \sim \frac{e^{-\frac{s^2}{2}}}{\sqrt{2\pi T}} \left[\rho + \sum_{k=3}^S T^{-\frac{k}{2}} \alpha_k \psi_k(s) \right], \quad (1.16)$$

where $\psi_k(s)$ is the Hermite polynomial of degree k and $\underline{\alpha}$ are coefficients chosen so that $\tilde{f}(s)$ matches the first $S+1$ input moments.

Maximum entropy closure: The maximum entropy closure [12, 28, 32] and its numerous variants (e.g., see [1, 2]) formulate the moment-inversion problem as an optimization problem to maximize the entropy under some assumed form of the distribution function. In the original formulation, the distribution function is approximated as an exponential of a polynomial:

$$\tilde{f}(s) \sim e^{\underline{\alpha} \cdot \underline{\Phi}(s)} \quad \text{where} \quad \underline{\Phi}(s) = [1, s, s^2, \dots]^T, \quad (1.17)$$

and the coefficients, $\underline{\alpha}$, are chosen so that $\tilde{f}(s)$ matches the first $S+1$ input moments.

Quadrature-based moment closures: In the quadrature-based method of moments (QMOM) [11, 15, 16, 29], the distribution function is represented as a sum of Dirac delta functions. This closure will be discussed in detail in §2.

1.4 Scope of this Work

In this work we study a particular five-moment moment-closure known as the hyperbolic quadrature-based moment closure (HyQMOM), which is originally due to Fox, Laurent, and Vié [17]. We begin in §2 with a review of the classical quadrature-based moment closure (QMOM), show its shortcomings, and then establish that the HyQMOM system is moment-invertible over a convex set in solution space. In §3 we introduce a novel high-order Lax-Wendroff discontinuous Galerkin scheme for solving the HyQMOM fluid system. The scheme is based on a predictor-corrector approach, where the prediction step is based on a localized space-time discontinuous Galerkin scheme. The nonlinear algebraic system that arises in this prediction step is solved using a Picard iteration. The correction step is a straightforward explicit update using the predicted solution in order to evaluate space-time flux integrals. In the absence of additional limiters, the proposed high-order scheme does not in general guarantee that the numerical solution remains in the convex set over which HyQMOM is moment-invertible. To overcome this challenge, we introduce in §4 novel limiters that rigorously guarantee that the computed solution does not leave the convex set over which moment-invertible and hyperbolicity of the fluid system is guaranteed. In particular, we develop positivity-preserving limiters in both the prediction and correction steps, as well as an oscillation-limiter that damps unphysical oscillations near shocks and rarefactions. Finally, in §5 we perform convergence tests to verify the order of

accuracy of the scheme, as well as test the scheme on Riemann data to demonstrate the shock-capturing and robustness of the method. Conclusions are provided in §6.

2 Quadrature-Based Moment Closures (QMOM)

In this section we review the quadrature-based moment-closure (QMOM) approach and describe in detail the five-moment hyperbolic regularization of QMOM (HyQMOM), which is the main focus of the current work.

2.1 Classical QMOM Approach

The classical quadrature-based moment-closure (QMOM) approach is widely used in modeling multiphase flows; key developments in this methodology have been developed over the course of the past several years, e.g., see [8, 11, 14, 15, 16, 29, 41].

The key idea is to assume that the distribution is a sum of Dirac delta functions whose locations (abscissas) and strengths (weights) are free parameters:

$$f(t, x, v) \approx f^\star(t, x, v) := \sum_{k=1}^N \omega_k \delta(v - \mu_k), \quad (2.1)$$

where $\delta(v)$ is the Dirac delta, and the quadrature weights, ω_k , and abscissas, μ_k , are all functions of t and x . This approach is reminiscent of other discrete velocity models such as the Broadwell model [3, 4, 34]; however, a key difference is that the discrete velocities, μ_k , change with the solution.

2.1.1 Example: $N = 2$ case

As a simple example, let us consider the $N = 2$ case. The first four moments of f^\star in (2.1) with $N = 2$ are

$$M_\ell = \omega_1 \mu_1^\ell + \omega_2 \mu_2^\ell \quad \text{for } \ell = 0, 1, 2, 3. \quad (2.2)$$

The moment inversion problem is then this: given (M_0, M_1, M_2, M_3) , find the parameters $(\mu_1, \mu_2, \omega_1, \omega_2)$ such that (2.2) is satisfied.

This inversion problem is equivalent to finding the quadrature points and weights for the following weighted Gaussian quadrature rule:

$$\int_{-\infty}^{\infty} g(v) f(v) dv \approx \omega_1 g(\mu_1) + \omega_2 g(\mu_2), \quad (2.3)$$

where $f(v)$ is a probability density function with moments (M_0, M_1, M_2, M_3) . If we attempt to make this quadrature rule exact with $g(v) = 1, v, v^2$, and v^3 , we again arrive at (2.2).

To find the correct Gaussian quadrature rule, we invoke results from classical numerical analysis and look for polynomials of degree up to two that are orthogonal

in the weighted $L^2(-\infty, \infty)$ inner product: $\langle \cdot, \cdot \rangle_f$. Such polynomials are easily obtained via Gram-Schmidt, and indeed the relevant one here is the quadratic polynomial:

$$\psi_2(v) = p^2 - p\rho(v-u)^2 + \rho q(v-u), \quad (2.4)$$

where ρ, u, p , and q are defined by (1.7)–(1.8). The abscissas are the two distinct real roots of $\psi_2(v)$ and the weights can easily be obtained by enforcing (2.2):

$$\mu_1, \mu_2 = u + \frac{q}{2p} \mp \sqrt{\frac{p}{\rho} + \left(\frac{q}{2p}\right)^2}, \quad \omega_1, \omega_2 = \frac{\rho}{2} \left[1 \pm \frac{\left(\frac{q}{2p}\right)}{\sqrt{\frac{p}{\rho} + \left(\frac{q}{2p}\right)^2}} \right]. \quad (2.5)$$

2.1.2 Weak hyperbolicity and linear degeneracy of QMOM

Theorem 2.1 (Weak hyperbolicity and linear degeneracy of QMOM) *The classical quadrature-based moment (QMOM) closure leads to a system of partial differential equations that has the following quasilinear form:*

$$\underline{q}_{,t} + \underline{A}(\underline{q}) \underline{q}_{,x}, \quad \text{where } \underline{q} = [M_0, M_1, \dots, M_{2N-2}, M_{2N-1}], \quad (2.6)$$

where the flux Jacobian matrix is given by

$$\underline{A}(\underline{q}) = \begin{bmatrix} 0 & 1 & & & \\ & 0 & 1 & & \\ & & \ddots & \ddots & \\ & & & 0 & 1 \\ \frac{\partial M_{2N}}{\partial M_0} & \frac{\partial M_{2N}}{\partial M_1} & \dots & \frac{\partial M_{2N}}{\partial M_{2N-2}} & \frac{\partial M_{2N}}{\partial M_{2N-1}} \end{bmatrix}. \quad (2.7)$$

System (2.6) and (2.7) is weakly hyperbolic for any integer $N \geq 1$ with the following properties:

1. The eigenvalues of (2.7) are $\lambda_k = \mu_k$ for $k = 1, 2, 3, \dots, N$, where μ_k are the abscissas in (2.1);
2. Every eigenvalue has algebraic multiplicity exactly two;
3. Every eigenvalue has geometric multiplicity exactly one; and
4. Every wave in the system is linearly degenerate: $\underline{\nabla}_q \lambda_k \cdot \underline{r}_k = 0$.

Proof The key to understanding the eigenvalues of flux Jacobian (2.7) is to understand the last row. To this end, consider:

$$M_{2N} = \sum_{k=1}^N \omega_k \mu_k^{2N} \implies \frac{\partial M_{2N}}{\partial M_\ell} = \sum_{k=1}^N \left[\mu_k^{2N} \frac{\partial \omega_k}{\partial M_\ell} + 2N \omega_k \mu_k^{2N-1} \frac{\partial \mu_k}{\partial M_\ell} \right]. \quad (2.8)$$

To make sense of this we need to obtain expressions for the partial derivatives of the quadrature weights and abscissas with respect to the moments. To this end, we compute the related quantities:

$$M_p = \sum_{k=1}^N \omega_k \mu_k^p \implies \frac{\partial M_p}{\partial M_\ell} = \sum_{k=1}^N \left[\mu_k^p \frac{\partial \omega_k}{\partial M_\ell} + p \omega_k \mu_k^{p-1} \frac{\partial \mu_k}{\partial M_\ell} \right] = \delta_\ell^p, \quad (2.9)$$

where $p, \ell = 0, 1, \dots, 2N-1$ and δ_ℓ^p is the Kronecker delta, which arises due to the fact that M_ℓ and M_p are independent variables if $p \neq \ell$. The expression in (2.9) can be written in matrix form to obtain the following result:

$$\begin{bmatrix} \frac{\partial \omega_1}{\partial M_0} & \cdots & \frac{\partial \omega_1}{\partial M_{2N-1}} \\ \vdots & & \vdots \\ \frac{\partial \omega_N}{\partial M_0} & \cdots & \frac{\partial \omega_N}{\partial M_{2N-1}} \\ \omega_1 \frac{\partial \mu_1}{\partial M_0} & \cdots & \omega_1 \frac{\partial \mu_1}{\partial M_{2N-1}} \\ \vdots & & \vdots \\ \omega_N \frac{\partial \mu_N}{\partial M_0} & \cdots & \omega_N \frac{\partial \mu_N}{\partial M_{2N-1}} \end{bmatrix}^T = \begin{bmatrix} 1 & \mu_1 & \mu_1^2 & \cdots & \mu_1^{2N-1} \\ \vdots & \vdots & \vdots & & \vdots \\ 1 & \mu_N & \mu_N^2 & \cdots & \mu_N^{2N-1} \\ 0 & 1 & 2\mu_1 & \cdots & (2N-1)\mu_1^{2N-2} \\ \vdots & \vdots & \vdots & & \vdots \\ 0 & 1 & 2\mu_N & \cdots & (2N-1)\mu_N^{2N-2} \end{bmatrix}^{-1}. \quad (2.10)$$

Using this result in (2.8) produces expressions for the last row of flux Jacobian (2.7):

$$\begin{bmatrix} \frac{\partial M_{2N}}{\partial M_0} \\ \frac{\partial M_{2N}}{\partial M_1} \\ \frac{\partial M_{2N}}{\partial M_2} \\ \vdots \\ \frac{\partial M_{2N}}{\partial M_{2N-2}} \\ \frac{\partial M_{2N}}{\partial M_{2N-1}} \end{bmatrix} = \begin{bmatrix} 1 & \mu_1 & \cdots & \mu_1^{2N-1} \\ \vdots & \vdots & & \vdots \\ 1 & \mu_N & \cdots & \mu_N^{2N-1} \\ 0 & 1 & \cdots & (2N-1)\mu_1^{2N-2} \\ \vdots & \vdots & & \vdots \\ 0 & 1 & \cdots & (2N-1)\mu_N^{2N-2} \end{bmatrix}^{-1} \begin{bmatrix} \mu_1^{2N} \\ \vdots \\ \mu_N^{2N} \\ 2N\mu_1^{2N-1} \\ \vdots \\ 2N\mu_N^{2N-1} \end{bmatrix} = \begin{bmatrix} a_0 \\ \vdots \\ a_{N-1} \\ a_N \\ \vdots \\ a_{2N-1} \end{bmatrix}, \quad (2.11)$$

where the last equality follows from Lemma A.1 and a_j for $j = 0, 1, \dots, 2N-1$ are the coefficients of the Hermite interpolating polynomial defined through (A.1) and (A.2).

Next we attempt to directly compute the eigenvalues of the flux Jacobian:

$$\left| \underline{\underline{A}} - v \underline{\underline{I}} \right| = \begin{vmatrix} -v & 1 & & & \\ & \ddots & \ddots & & \\ & & -v & & 1 \\ a_0 & \cdots & a_{2N-2} & (a_{2N-1} - v) \end{vmatrix} = v^{2N} - \sum_{k=0}^{2N-1} a_k v^k. \quad (2.12)$$

Using a classical result from Hermite polynomial interpolation, we can write the right-most term in the above expression as follows (e.g., see Theorem 6.4 on page 190 of Süli and Mayer [39]):

$$\left| \underline{\underline{A}} - v \underline{\underline{I}} \right| = (v - \mu_1)^2 (v - \mu_2)^2 \cdots (v - \mu_N)^2. \quad (2.13)$$

This proves the first two claims of the theorem: (1) the eigenvalues are the quadrature abscissas, and (2) each eigenvalue has algebraic multiplicity exactly two.

Next we look at the eigenvectors. For example, the k^{th} eigenvector for each $k = 1, 2, \dots, N$ satisfies the relationship:

$$\left(\underline{A} - \mu_k \underline{\mathbb{I}}\right) \underline{r}^k = \underline{0}. \quad (2.14)$$

By inspection, we see that $\underline{r}^k \neq \underline{0}$ if and only if the first component of \underline{r}^k is not zero. Without loss of generality the first component is taken to be unity, and then by inspection we note that the only eigenvector associated to eigenvalue $v = \mu_k$ must be

$$\underline{r}^k = \left(1, \mu_k, \mu_k^2, \dots, \mu_k^{2N-1}\right)^T. \quad (2.15)$$

This proves the third claim of the theorem: (3) each eigenvalue has geometric multiplicity exactly one. Since the geometric multiplicity for each eigenvalue is strictly less than the algebraic multiplicity, system (2.6) and (2.7) is weakly hyperbolic for any integer $N \geq 1$.

The final claim in the theorem is that each wave is linearly degenerate. Proving this requires us to investigate the following dot product

$$\nabla_q \mu_k \cdot \underline{r}^k. \quad (2.16)$$

Invoking Lemmas (A.2) and (A.3) shows that for every $k = 1, 2, \dots, N$:

$$\nabla_q \mu_k \cdot \underline{r}^k = \lim_{s \rightarrow \mu_k} \left\{ \frac{(s - \mu_k)}{\omega_k} \left[\prod_{\substack{p=1 \\ p \neq k}}^N (s - \mu_p)^2 \right] \left/ \prod_{\substack{p=1 \\ p \neq k}}^N (\mu_k - \mu_p)^2 \right. \right] \right\} = 0, \quad (2.17)$$

which proves that every wave for $k = 1, 2, \dots, N$ is linearly degenerate. ■

2.2 Pressure Regularized QMOM

In order to overcome the weak hyperbolicity present in classical QMOM, Chalons, Fox, and Massot [7] proposed to replace the delta function ansatz (2.1) with a multi-Gaussian ansatz of the form:

$$f(t, x, v) \approx f^\star(t, x, v) := \frac{1}{\sqrt{2\pi}\sigma} \sum_{k=1}^N \omega_k \exp \left[-\frac{(v - \mu_k)^2}{2\sigma} \right], \quad (2.18)$$

where the free parameters are now the quadrature weights, ω_k , the abscissas, μ_k , and the additional parameter σ . A similar approach using B-splines was also considered by Cheng and Rossmanith [9]. The additional parameter σ allows this closure to match an additional moment (i.e., a total of $2N + 1$ moments can now be matched), but more importantly, it provides a pressure regularization that restores strong hyperbolicity. Unfortunately, this closure exhibits a singularity in the limit of thermodynamic

equilibrium, since in that limit all the quadrature points collapse to the macroscopic velocity:

$$\sigma \rightarrow T, \quad \sum_{k=1}^N \omega_k = \rho, \quad \text{and} \quad \mu_k \rightarrow u \quad \forall k \in [1, N]. \quad (2.19)$$

This type of singularity is also evident in other closures, most notably the *maximum entropy* closure [22].

2.3 HyQMOM: Density Regularized QMOM

As an alternative to the above described pressure regularized QMOM, Fox et al. [17, 33] developed a density regularized version, which they refer to as HyQMOM (hyperbolic quadrature-based method of moments). This approach was also studied by Johnson [21] and Wiersma [42]. The five-moment HyQMOM system is the subject of the current work and we briefly review it in this section.

The idea of HyQMOM is as follows: again approximate the distribution as a sum of delta functions (as in classical QMOM), but place one (or more) of these delta functions at known locations. This converts the quadrature rule from classical Gaussian quadrature to something akin to Gauss-Radau quadrature. The version of this idea relevant to the current work is the case of three delta functions:

$$f \approx f^\star = \omega_1 \delta(v - \mu_1) + \omega_2 \delta(v - u) + \omega_3 \delta(v - \mu_3), \quad (2.20)$$

where two of the delta distributions are at unknown locations μ_1, μ_3 and the last delta distribution is fixed at the velocity, u . Each of the distributions is weighted by $\omega_1, \omega_2, \omega_3$. This results in the following moment-inversion problem:

$$\begin{aligned} \omega_1 + \omega_3 &= \tilde{\rho}, \\ \omega_1 \mu_1 + \omega_3 \mu_3 &= \tilde{\rho} u, \\ \omega_1 \mu_1^2 + \omega_3 \mu_3^2 &= \tilde{\rho} u^2 + p, \\ \omega_1 \mu_1^3 + \omega_3 \mu_3^3 &= \tilde{\rho} u^3 + 3pu + q, \end{aligned} \quad (2.21)$$

and

$$\tilde{\rho} := \rho - \omega_2 = \omega_1 \left(\frac{\mu_1}{u} \right)^4 + \omega_3 \left(\frac{\mu_3}{u} \right)^4 - \frac{6\rho p^2 u^2 + 4\rho p q u + p^3 + \rho q^2 + \rho p k}{\rho p u^4}. \quad (2.22)$$

System (2.21) can be solved in the same way that the $N = 2$ classical QMOM system was solved, namely by constructing a quadratic orthogonal polynomial:

$$\psi_2(v) = p^2 - p\tilde{\rho}(v - u)^2 + q\tilde{\rho}(v - u), \quad (2.23)$$

which is just (2.4) with $\rho \rightarrow \tilde{\rho}$. The roots of (2.23) provide μ_1 and μ_3 , and the corresponding weights, ω_1 and ω_3 , can easily be computed from (2.21) once μ_1 and

μ_3 are known:

$$\mu_1, \mu_3 = u + \frac{q}{2p} \mp \sqrt{\frac{p}{\tilde{\rho}} + \left(\frac{q}{2p}\right)^2}, \quad \omega_1, \omega_3 = \frac{\tilde{\rho}}{2} \left[1 \pm \frac{\left(\frac{q}{2p}\right)}{\sqrt{\frac{p}{\tilde{\rho}} + \left(\frac{q}{2p}\right)^2}} \right]. \quad (2.24)$$

Finally, we can obtain ω_2 and fully solve the moment inversion problem by inserting the above expressions for $\omega_1, \omega_3, \mu_1$, and μ_3 into (2.22):

$$\tilde{\rho} = \rho - \omega_2 = \frac{p^3}{p \left(k + \frac{p^2}{\rho} + \frac{q^2}{p} \right) - q^2}. \quad (2.25)$$

Putting all of these results together yields:

$$M_5^* = \rho u^5 + 10pu^3 + 10qu^2 + 5ru + \frac{2qr}{p} - \frac{q^3}{p^2}, \quad \text{where } r := \frac{p^2}{\rho} + \frac{q^2}{p} + k. \quad (2.26)$$

From this we can now assemble the full fluid approximation implied by the 5-moment HyQMOM approximation (2.20).

Definition 2.1 (5-moment HyQMOM fluid approximation) The 5-moment HyQMOM approximation can be written either in conservative or primitive form:

$$\underline{q}_{,t} + \underline{f}(\underline{q})_{,x} = \underline{0} \quad \text{or} \quad \underline{\alpha}_{,t} + \underline{B}(\underline{\alpha}) \underline{\alpha}_{,x} = \underline{0}, \quad (2.27)$$

respectively, where

$$\underline{q} = \begin{bmatrix} \rho \\ \rho u \\ \rho u^2 + p \\ \rho u^3 + 3pu + q \\ \rho u^4 + 6pu^2 + 4qu + r \end{bmatrix}, \quad \underline{f}(\underline{q}) = \begin{bmatrix} \rho u \\ \rho u^2 + p \\ \rho u^3 + 3pu + q \\ \rho u^4 + 6pu^2 + 4qu + r \\ M_5^* \end{bmatrix}, \quad (2.28)$$

where r and M_5^* are defined by (2.26), and

$$\underline{\alpha} = \begin{bmatrix} \rho \\ u \\ p \\ q \\ k \end{bmatrix}, \quad \underline{B}(\underline{\alpha}) = \begin{bmatrix} u & \rho & 0 & 0 & 0 \\ 0 & u & \frac{1}{\rho} & 0 & 0 \\ 0 & 3p & u & 1 & 0 \\ -\frac{p^2}{\rho^2} & 4q & -\frac{q^2}{p^2} - \frac{p}{\rho} & u + \frac{2q}{p} & 1 \\ 0 & 5k & -\frac{2kq}{p^2} & \frac{2k}{p} & u \end{bmatrix}. \quad (2.29)$$

Furthermore, we note that that conservative flux Jacobian has the following form:

$$\underline{A}(\underline{q}) := \underline{f}(\underline{q})_{,q} = \begin{bmatrix} 0 & 1 & 0 & 0 & 0 \\ 0 & 0 & 1 & 0 & 0 \\ 0 & 0 & 0 & 1 & 0 \\ 0 & 0 & 0 & 0 & 1 \\ \frac{\partial M_5^*}{\partial M_0} & \frac{\partial M_5^*}{\partial M_1} & \frac{\partial M_5^*}{\partial M_2} & \frac{\partial M_5^*}{\partial M_3} & \frac{\partial M_5^*}{\partial M_4} \end{bmatrix}, \quad (2.30)$$

where the details of the last row have been omitted for brevity. The matrices \underline{A} and \underline{B} as defined in (2.30) and (2.29), respectively, are *similar matrices*, meaning that they share the same eigenvalues.

Proposition 2.1 (Hyperbolicity of HyQMOM) *The HyQMOM fluid model as expressed either in conservative or primitive form (2.27)–(2.29) is strictly hyperbolic for all $\rho, p, k > 0$. The resulting wave structure includes one linearly degenerate wave and four nonlinear waves.*

Proof The eigenvalues of the Jacobian matrix, $\underline{B}(\underline{\alpha})$, in (2.29) can be computed explicitly:

$$\begin{aligned}\lambda_1 &= u + \frac{q}{2p} - \sqrt{a+b}, & \lambda_2 &= u + \frac{q}{2p} - \sqrt{a-b}, & \lambda_3 &= u, \\ \lambda_4 &= u + \frac{q}{2p} + \sqrt{a-b}, & \lambda_5 &= u + \frac{q}{2p} + \sqrt{a+b},\end{aligned}\quad (2.31)$$

where

$$a = \frac{p}{\rho} + \frac{k}{p} + \left(\frac{q}{2p}\right)^2 \quad \text{and} \quad b = \sqrt{\frac{k^2}{p^2} + \frac{k}{\rho}}. \quad (2.32)$$

One can show via simple calculations that for all $\rho, p, k > 0$:

$$a > b > 0, \quad \sqrt{a+b} > \frac{|q|}{2p}, \quad \text{and} \quad \sqrt{a-b} > \frac{|q|}{2p}. \quad (2.33)$$

Therefore, all five eigenvalues shown in (2.31)–(2.32) are real and distinct for all $\rho, p, k > 0$, which is sufficient to show that system (2.27)–(2.29) is a strictly hyperbolic.

The eigenvectors of the flux Jacobian (2.30) can be written as follows:

$$\underline{r}_\ell = [1, \lambda_\ell, \lambda_\ell^2, \lambda_\ell^3, \lambda_\ell^4]^T \quad \text{for} \quad \ell = 1, 2, 3, 4, 5. \quad (2.34)$$

In order to determine whether the corresponding waves are linearly degenerate or not, we need to compute the quantities:

$$\frac{\partial \lambda_\ell}{\partial \underline{q}} \cdot \underline{r}_\ell = \frac{\partial \lambda_\ell}{\partial \underline{\alpha}} \cdot \left(\frac{\partial \underline{q}}{\partial \underline{\alpha}} \right)^{-1} \cdot \underline{r}_\ell, \quad (2.35)$$

for each $\ell = 1, 2, 3, 4, 5$, where

$$\frac{\partial \underline{q}}{\partial \underline{\alpha}} = \begin{bmatrix} 1 & 0 & 0 & 0 & 0 \\ u & \rho & 0 & 0 & 0 \\ u^2 & 2\rho u & 1 & 0 & 0 \\ u^3 & 3(p + \rho u^2) & 3u & 1 & 0 \\ \frac{\rho^2 u^4 - p^2}{\rho^2} & 4(q + 3pu + \rho u^3) & \frac{6\rho p^2 u^2 + 2p^3 - \rho q^2}{\rho p^2} & \frac{2q + 4pu}{p} & 1 \end{bmatrix}. \quad (2.36)$$

We note that one of the waves is linearly degenerate, while the remaining are nonlinear:

$$\frac{\partial \lambda_3}{\partial \underline{q}} \cdot \underline{r}_3 \equiv 0 \quad \text{and} \quad \frac{\partial \lambda_\ell}{\partial \underline{q}} \cdot \underline{r}_\ell \not\equiv 0 \quad \text{for} \quad \ell = 1, 2, 4, 5. \quad (2.37)$$

■

3 Locally-implicit Lax-Wendroff discontinuous Galerkin

We consider generic one-dimensional conservation laws of the form:

$$\underline{q}_{,t} + \underline{f}(\underline{q})_{,x} = 0, \quad (3.1)$$

where t is time, x is space, $q(t, x) : \mathbb{R}^+ \times \mathbb{R} \mapsto \mathbb{R}^{M_{\text{eqn}}}$ is the vector of conserved variables, M_{eqn} is the number of equations, and $\underline{f}(\underline{q}) : \mathbb{R}^{M_{\text{eqn}}} \mapsto \mathbb{R}^{M_{\text{eqn}}}$ is the flux function. We assume that this system is hyperbolic, meaning that the flux Jacobian:

$$\underline{f}(\underline{q})_{,q} : \mathbb{R}^{M_{\text{eqn}}} \mapsto \mathbb{R}^{M_{\text{eqn}} \times M_{\text{eqn}}}, \quad (3.2)$$

has real eigenvalues and a complete set of eigenvectors over some convex region $\mathcal{D} \subset \mathbb{R}^{M_{\text{eqn}}}$ in solution space inside of which we are interested in solving the equation.

The Lax-Wendroff method [26] is a time discretization for hyperbolic conservation laws based on the the Cauchy-Kovalevskaya [25] procedure to convert temporal derivatives into spatial derivatives. We begin with a Taylor series in time:

$$\underline{q}(t + \Delta t, x) = \underline{q}(t, x) + \Delta t \underline{q}_{,t}(t, x) + \frac{1}{2} \Delta t^2 \underline{q}_{,t,t}(t, x) + \dots, \quad (3.3)$$

and then replace all time derivatives by spatial derivatives:

$$\underline{q}_{,t} = -\underline{f}(\underline{q})_{,x}, \quad \underline{q}_{,t,t} = -\underline{f}(\underline{q})_{,t,x} = -\left[\underline{f}'(\underline{q}) \underline{q}_{,t} \right]_{,x} = \left[\underline{f}'(\underline{q}) \underline{f}(\underline{q})_{,x} \right]_{,x}, \quad \dots, \quad (3.4)$$

which results in the following:

$$\underline{q}(t + \Delta t, x) = \underline{q} - \Delta t \underline{f}(\underline{q})_{,x} + \frac{1}{2} \Delta t^2 \left[\underline{f}'(\underline{q}) \underline{f}(\underline{q})_{,x} \right]_{,x} + \dots, \quad (3.5)$$

where on the right-hand side we have suppressed the evaluation at (t, x) . The final step is to truncate the Taylor series at some finite number of terms, and then replace all spatial derivatives by some discrete spatial derivative operators. The above Lax-Wendroff formalism [26] has been used in conjunction with a variety of spatial discretizations, including finite volume [27], weighted essentially non-oscillatory (WENO) [40], and discontinuous Galerkin [35] operators.

In this work, we are concerned with the discontinuous Galerkin version of Lax-Wendroff [35]; and in particular, we make use of the reformulation of Gassner et al. [18] of the Lax-Wendroff discontinuous Galerkin (LxW-DG) scheme in terms of a locally-implicit prediction step, followed by an explicit correction step. The key advantage of this formulation is that we do not need to explicitly compute the partial derivatives as shown in (3.4); and instead, the locally-implicit solver automatically produces discrete versions of these derivatives. The next challenge is to efficiently solve the nonlinear algebraic equations that arise from the locally-implicit prediction step; we solve these equations by again following Gassner et al. [18] and making use of a Picard fixed point iteration. We will follow the notational conventions of Guthrey and Rossmanith [20] developed for locally-implicit and regionally-implicit LxW-DG schemes.

3.1 Discontinuous Galerkin Method

To discretize equation (3.1) in space we use the discontinuous Galerkin (DG) finite element method, which was first introduced by Reed and Hill [36]. It was fully developed for time-dependent hyperbolic conservation laws in a series of papers by Bernardo Cockburn, Chi-Wang Shu, and collaborators (see [10] and references therein for details).

We define the broken finite element space

$$\mathcal{W}^h := \{w^h \in [L^\infty(\Omega)]^{M_{\text{eqn}}} : w^h|_{\mathcal{T}_i} \in [\mathbb{P}(M_{\text{deg}})]^{M_{\text{eqn}}} \quad \forall \mathcal{T}_i\}, \quad (3.6)$$

where $h = \Delta x = (x_{\text{high}} - x_{\text{low}})/M_{\text{elem}}$ is a uniform grid spacing with M_{elem} being the number of elements. Additionally, M_{eqn} is the number of conserved variables, M_{deg} is the maximal polynomial degree, and the computational mesh is described by non-overlapping elements of width Δx centered at the points x_i :

$$\mathcal{T}_i = \left[x_i - \frac{\Delta x}{2}, x_i + \frac{\Delta x}{2} \right] \quad \text{for } i = 1, \dots, M_{\text{elem}}. \quad (3.7)$$

On each element we define the local spatial variable, ξ :

$$x = x_i + \left(\frac{\Delta x}{2} \right) \xi \quad \text{for } \xi \in [-1, 1]. \quad (3.8)$$

On each element we approximate the solution by a finite expansion in terms of the following orthonormal Legendre polynomial basis functions:

$$\underline{\Phi} = \left(1, \sqrt{3}\xi, \frac{\sqrt{5}}{2}(3\xi^2 - 1), \frac{\sqrt{7}}{2}(5\xi^3 - 3\xi), \frac{\sqrt{9}}{8}(35\xi^4 - 30\xi^2 + 3), \dots \right), \quad (3.9)$$

with the orthonormality property:

$$\frac{1}{2} \int_{-1}^1 \underline{\Phi} \underline{\Phi}^T d\xi = \mathbb{I}, \quad (3.10)$$

where \mathbb{I} is the identity matrix. On each element at time $t = t^n$, we approximate the solution as follows:

$$\underline{q}^h \left(t^n, x_i + \frac{\Delta x}{2} \xi \right) := \underline{\Phi}(\xi)^T \underline{\underline{Q}}_i^n \quad \text{for } \xi \in [-1, 1], \quad (3.11)$$

where

$$\underline{\Phi}(\xi) : [-1, 1] \mapsto \mathbb{R}^{M_C} \quad \text{and} \quad \underline{\underline{Q}}_i^n \in \mathbb{R}^{M_C \times M_{\text{eqn}}}. \quad (3.12)$$

The number of basis functions in 1D is $M_C = M_{\text{deg}} + 1$, and the order of accuracy is $M_O = M_{\text{deg}} + 1$.

3.2 Prediction Step

The prediction step is completely local on each element; and as such, the prediction step by itself is not consistent with the underlying conservation law. This inconsistency allows us freedom in the choice of variables that are updated; we choose to use the primitive variables for this step: $\underline{\alpha} = (\rho, u, p, q, k)$.

The prediction step is local on each space-element $[t^n, t^{n+1}] \times \mathcal{T}_i$, where $t^{n+1} = t^n + \Delta t$. Let $t = t^n + \frac{\Delta t}{2}(1 + \tau)$, for $\tau \in [-1, 1]$ and

$$\underline{\alpha}_{,\tau} = \underline{\Theta}(\underline{\alpha}) := -\frac{\Delta t}{\Delta x} \underline{B}(\underline{\alpha}) \underline{\alpha}_{,\xi}, \quad (3.13)$$

where $\underline{B}(\underline{\alpha})$ is the (primitive variable) flux Jacobian matrix defined by (2.29). We introduce a space-time Legendre basis on each element:

$$\Psi_\ell(\tau, \xi) = \Phi_{\ell_1}(\tau) \Phi_{\ell_2}(\xi), \quad \text{for } \ell_1 = 1, \dots, M_O, \quad \ell_2 = 1, \dots, M_O + 1 - \ell_1, \quad (3.14)$$

where

$$\ell = M_O(\ell_1 - 1) - \frac{(\ell_1 - 1)(\ell_1 - 2)}{2} + \ell_2 \quad \text{such that } \ell = 1, \dots, M_P, \quad (3.15)$$

and $M_P = M_O(M_O + 1)/2$ is the number of space-time basis functions. These space-time basis functions are orthonormal on $[-1, 1]^2$:

$$\frac{1}{4} \int_{-1}^1 \int_{-1}^1 \underline{\Psi} \underline{\Psi}^T d\tau d\xi = \mathbb{I}. \quad (3.16)$$

We write the predicted solution as:

$$\underline{\alpha}^{\text{ST}} \left(t^n + \frac{\Delta t}{2}(1 + \tau), x_i + \frac{\Delta x}{2} \xi \right) := \underline{\Psi}(\tau, \xi)^T \underline{W}_i^{n+\frac{1}{2}}, \quad \underline{W}_i^{n+\frac{1}{2}} \in \mathbb{R}^{M_P \times M_{\text{eqn}}}, \quad (3.17)$$

for $(\tau, \xi) \in [-1, 1]^2$, where \underline{W} represents the matrix of unknown coefficients.

We proceed by multiplying (3.13) by the test function $\underline{\Psi}$, then integrating over $(\tau, \xi) \in [-1, 1]^2$, and finally applying integration-by-parts in τ only. The end result is

$$\begin{aligned} \underline{L} \underline{W}_i^{n+\frac{1}{2}} = & \frac{1}{4} \int_{-1}^1 \int_{-1}^1 \underline{\Theta}_m \left(\underline{\Psi}^T \underline{W}_i^{n+\frac{1}{2}} \right) \underline{\Psi} d\tau d\xi \\ & + \left[\frac{1}{4} \int_{-1}^1 \underline{\Psi}(-1, \xi) \underline{\Phi}(\xi)^T d\xi \right] \underline{A}_i^{n+1}, \end{aligned} \quad (3.18)$$

for each equation $m = 1, \dots, M_{\text{eqn}}$, where

$$\underline{L} = \frac{1}{4} \int_{-1}^1 \int_{-1}^1 \underline{\Psi} \underline{\Psi}_{,\tau}^T d\tau d\xi + \frac{1}{4} \int_{-1}^1 \underline{\Psi}_{|\tau=-1} \underline{\Psi}_{|\tau=-1}^T d\xi, \quad (3.19)$$

$$\underline{A}_i^n = \frac{1}{2} \sum_{a=1}^{M_O} \omega_a \underline{\Phi}(\mu_a) \left[\underline{\alpha} \left(\underline{\Phi}(\mu_a)^T \underline{Q}_i^n \right) \right]^T, \quad (3.20)$$

and $\underline{\alpha}(q)$ gives the relationship between conservative and primitive variables. Equation (3.18) is a nonlinear algebraic equation that must be solved on each space-time element for the matrix of unknown coefficients: \underline{W} .

Following Gassner et al. [18], instead of using Newton's method to solve the resulting non-linear equation, which involves inverting a Jacobian matrix at every step, we used the much simpler Picard iteration. There are two key advantages of the Picard iteration over Newton's method. First, since \underline{L} is independent of the solution and the same on each space-time element, we only invert this relatively small matrix once. Second, the Picard iteration converges to sufficiently high order accuracy after $M_O - 1$ iterations, so the need to compute residuals is eliminated. We can write the Picard iteration as

$$\begin{aligned} \underline{W}_{i(:,m)}^{n+\frac{1}{2}} \leftarrow & \frac{1}{4} \sum_{a=1}^{M_O} \sum_{b=1}^{M_O} \omega_a \omega_b \underline{\Psi}(\mu_b, \mu_a) \underline{\Theta}_m \left(\underline{\Psi}(\mu_b, \mu_a)^T \underline{W}_i^{n+\frac{1}{2}} \right) \\ & + \frac{1}{4} \sum_{b=1}^{M_O} \omega_b \underline{\Psi}(-1, \xi_b) \underline{\Phi}(\xi_b)^T \underline{A}_{i(:,m)}^n, \end{aligned} \quad (3.21)$$

for $m = 1, \dots, M_{\text{eqn}}$, where $\underline{\Psi} = \underline{L}^{-1} \underline{\Psi}$ and ω_a and μ_a for $a = 1, \dots, M_O$ are the weights and abscissas of the M_O -point Gauss-Legendre quadrature rule. This gives a solution for the prediction step, which we know is not consistent with the conservation law. In order to make the final solution consistent (and high-order) with the original conservation law, we next need to add a correction step.

3.3 Correction Step

The correction step is designed to work like a single forward Euler-like step that uses the predicted solution. To perform this step, we begin with the hyperbolic conservation law (3.1) and multiply by the spatial basis functions defined in (3.9). Next, we integrate over the space-time element $(\tau, \xi) \in [-1, 1]^2$:

$$\frac{1}{2} \int_{-1}^1 \int_{-1}^1 \left[\underline{\Phi}(\xi) \underline{q}_{,\tau} + \nu \underline{\Phi}(\xi) \underline{f}(\underline{q})_{,\xi} \right] d\xi d\tau = \underline{0}, \quad (3.22)$$

which can be written as

$$\begin{aligned} \frac{1}{2} \int_{-1}^1 \underline{\Phi}(\xi) \underline{q} \left(t^{n+1}, x_i + \frac{\Delta x}{2} \xi \right) d\xi &= \frac{1}{2} \int_{-1}^1 \underline{\Phi}(\xi) \underline{q} \left(t^n, x_i + \frac{\Delta x}{2} \xi \right) d\xi \\ &\quad - \frac{\nu}{2} \int_{-1}^1 \int_{-1}^1 \underline{\Phi}(\xi) \underline{f}(\underline{q})_{,\xi} d\xi d\tau, \end{aligned} \quad (3.23)$$

where $\nu = \Delta t / \Delta x$. We approximate $\underline{q}(t^{n+1}, \cdot)$ and $\underline{q}(t^n, \cdot)$ in (3.23) via appropriate versions of ansatz (3.11). For the remaining term, we first apply integration-by-parts

in space, then replace the true solution q by its space-time predicted solution: (3.17). This results in the following expression:

$$\begin{aligned}
\underline{\underline{Q}}_i^{n+1} &= \underline{\underline{Q}}_i^n + \frac{\nu}{2} \int_{\tau=-1}^{\tau=1} \int_{\xi=-1}^{\xi=1} \underline{\underline{\Phi}}_{,\xi} f\left(\underline{\underline{\Psi}}^T \underline{\underline{W}}_i^{n+\frac{1}{2}}\right) d\xi d\tau \\
&\quad - \nu \left(\underline{\underline{\Phi}}(1) \left[\underline{\underline{\mathcal{F}}}_{i+\frac{1}{2}}^{n+\frac{1}{2}} \right]^T - \underline{\underline{\Phi}}(-1) \left[\underline{\underline{\mathcal{F}}}_{i-\frac{1}{2}}^{n+\frac{1}{2}} \right]^T \right) \\
&\approx \underline{\underline{Q}}_i^n + \frac{\nu}{2} \sum_{a=1}^{M_0} \sum_{b=1}^{M_0} \omega_a \omega_b \underline{\underline{\Phi}}_{,\xi}(\mu_a) \left[f\left(\underline{\underline{\Psi}}(\mu_b, \mu_a)^T \underline{\underline{W}}_i^{n+\frac{1}{2}}\right) \right]^T \\
&\quad - \nu \left(\underline{\underline{\Phi}}(1) \left[\underline{\underline{\mathcal{F}}}_{i+\frac{1}{2}}^{n+\frac{1}{2}} \right]^T - \underline{\underline{\Phi}}(-1) \left[\underline{\underline{\mathcal{F}}}_{i-\frac{1}{2}}^{n+\frac{1}{2}} \right]^T \right),
\end{aligned} \tag{3.24}$$

where $\nu = \Delta t / \Delta x$. In the expressions after the approximation symbol, \approx , we replaced all exact integration by a Gauss-Legendre quadrature, where ω_a and μ_a for $a = 1, \dots, M_0$ are the weights and abscissas of the M_0 -point Gauss-Legendre quadrature rule.

The time-integrated numerical fluxes are defined using the predicted solution and the Rusanov [37] time-averaged flux:

$$\underline{\underline{\mathcal{F}}}_{i-\frac{1}{2}}^{n+\frac{1}{2}} := \frac{1}{2} \sum_{a=1}^{M_0} \omega_a \underline{\underline{\mathcal{F}}}(\mu_a), \tag{3.25}$$

where the numerical flux at each temporal quadrature point is given by

$$\underline{\underline{\mathcal{F}}}(\tau) := \frac{1}{2} \left\{ \underline{\underline{f}}\left(\underline{\underline{W}}_R(\tau)\right) + \underline{\underline{f}}\left(\underline{\underline{W}}_L(\tau)\right) \right\} - \frac{1}{2} \lambda_{\max}(\tau) \left\{ \underline{\underline{q}}\left(\underline{\underline{W}}_R(\tau)\right) - \underline{\underline{q}}\left(\underline{\underline{W}}_L(\tau)\right) \right\}, \tag{3.26}$$

where

$$\underline{\underline{W}}_L(\tau) := \underline{\underline{\Psi}}(\tau, 1)^T \underline{\underline{W}}_{i-1}^{n+\frac{1}{2}}, \quad \underline{\underline{W}}_R(\tau) := \underline{\underline{\Psi}}(\tau, -1)^T \underline{\underline{W}}_i^{n+\frac{1}{2}}, \tag{3.27}$$

and $\lambda_{\max}(\tau)$ is a local bound on the spectral radius of the flux Jacobian, $\underline{\underline{f}}(\underline{\underline{q}})_{,\underline{\underline{q}}} = \underline{\underline{A}}(\underline{\underline{q}})$, in the neighborhood of interface $x = x_{i-\frac{1}{2}}$ and at time $t = t^n + (\tau + 1)\Delta t/2$.

These steps are all it takes to regain the coupling that was neglected in the prediction step. In fact, we now have a solution which is not only consistent with the conservation law, but is also high order. We do however still have some work to do to ensure that the solution is physical. We must be careful to maintain the positivity of the primitive variables ρ , p , k , as was necessary for the hyperbolicity of the system and for moment-realizability. We address the limiters utilized to accomplish this in the next section.

4 Limiters

The high-order numerical method as described in §3 does not guarantee that density, pressure, and modified kurtosis remain positive over the course of a time-step:

$$\rho^n > 0, \quad p^n > 0, \quad k^n > 0 \quad \not\Rightarrow \quad \rho^{n+1} > 0, \quad p^{n+1} > 0, \quad k^{n+1} > 0. \quad (4.1)$$

Recall that positivity of these quantities is needed to guarantee moment-realizability of the moment-closure and strict hyperbolicity of the resulting evolution equations. If we want positivity over a time-step, we will need to introduce *positivity-preserving limiters*. Additionally, if we want to control unphysical oscillations near large gradients, shocks, and rarefactions, we will also need *non-oscillatory limiters*. In this section we derive all of these limiters. In particular, we first need to establish that a simple first-order scheme is positivity-preserving under some appropriate time-step restriction; this is done in §4.1. Using this result we derive a suite of limiters that ensure positivity: §4.2 (positivity at select points in the prediction step), §4.3 (positivity of the average density, pressure, and modified kurtosis in each element in the correction step), and §4.4 (positivity at select points in the correction step). We then develop an unphysical oscillation limiter in §4.5.

4.1 Positivity of the Rusanov scheme

Before considering positivity limiters for the high-order method, we must first establish that simple first-order schemes, in this case we consider the Rusanov (aka local Lax-Friedrichs) scheme [37], are positivity-preserving under some appropriate time-step restriction. This is established in the theorem below, which is an extension of the result of Zhang and Shu [44] for the compressible Euler equations.

Theorem 4.1 *Let $v = \Delta t / \Delta x$, let \underline{Q}_i^n be some approximation of the element averages of the conserved variables on element \mathcal{T}_i at time t^n , and let \underline{Q}_i^{n+1} the element averages of the conserved variables on element \mathcal{T}_i produced by the Rusanov scheme [37] at time $t^{n+1} = t^n + \Delta t$. Then*

$$\rho_i^n > 0, \quad p_i^n > 0, \quad k_i^n > 0 \quad \forall i \quad \implies \quad \rho_i^{n+1} > 0, \quad p_i^{n+1} > 0, \quad k_i^{n+1} > 0 \quad \forall i, \quad (4.2)$$

under the CFL condition:

$$v \cdot \max_i \left(\lambda_{i+\frac{1}{2}} \right) < 1, \quad (4.3)$$

where

$$\lambda_{i\pm\frac{1}{2}} = \max \left\{ \lambda_{\max} \left(\underline{Q}_i^n \right), \lambda_{\max} \left(\underline{Q}_{i\pm 1}^n \right), \lambda_{\max} \left(\frac{1}{2} \left(\underline{Q}_i^n + \underline{Q}_{i\pm 1}^n \right) \right) \right\}, \quad (4.4)$$

and $\lambda_{\max} \left(\underline{Q}_i^n \right)$ is a bound on the spectral radius of the flux Jacobian (2.30) at state \underline{Q}_i^n .

Proof Recall that the Rusanov scheme can be written as

$$\underline{Q}_i^{n+1} = \underline{Q}_i^n - \nu \left(\underline{\mathcal{F}}_{i+\frac{1}{2}} - \underline{\mathcal{F}}_{i-\frac{1}{2}} \right), \quad (4.5)$$

where the numerical fluxes are given by

$$\underline{\mathcal{F}}_{i\pm\frac{1}{2}} = \frac{1}{2} \left[\underline{f}(\underline{Q}_i^n) + \underline{f}(\underline{Q}_{i\pm 1}^n) \right] - \frac{1}{2} \lambda_{i\pm\frac{1}{2}} \left(\underline{Q}_i^n - \underline{Q}_{i\pm 1}^n \right), \quad (4.6)$$

where the flux function, $\underline{f}(\underline{q})$, is defined by (2.28) and the local wave speed, $\lambda_{i\pm\frac{1}{2}}$, is defined by (4.4). We can rewrite the above expression into the following numerical update:

$$\begin{aligned} \underline{Q}_i^{n+1} &= \underline{Q}_i^n - \frac{\nu}{2} \left[\underline{f}(\underline{Q}_{i+1}^n) - \underline{f}(\underline{Q}_{i-1}^n) - \lambda_{i+\frac{1}{2}} (\underline{Q}_{i+1}^n - \underline{Q}_i^n) + \lambda_{i-\frac{1}{2}} (\underline{Q}_i^n - \underline{Q}_{i-1}^n) \right] \\ &= \left[1 - \frac{\nu}{2} (\lambda_{i+\frac{1}{2}} + \lambda_{i-\frac{1}{2}}) \right] \underline{Q}_i^n + \left[\frac{\nu \lambda_{i+\frac{1}{2}}}{2} \right] \underline{M}_i^+ + \left[\frac{\nu \lambda_{i-\frac{1}{2}}}{2} \right] \underline{M}_i^-, \end{aligned} \quad (4.7)$$

where

$$\underline{M}_i^+ = \underline{Q}_{i+1}^n - \left(\lambda_{i+\frac{1}{2}} \right)^{-1} \underline{f}(\underline{Q}_{i+1}^n) \quad \text{and} \quad \underline{M}_i^- = \underline{Q}_{i-1}^n + \left(\lambda_{i-\frac{1}{2}} \right)^{-1} \underline{f}(\underline{Q}_{i-1}^n). \quad (4.8)$$

Under the CFL condition (4.3), we note that

$$1 - \frac{\nu}{2} (\lambda_{i+\frac{1}{2}} + \lambda_{i-\frac{1}{2}}) > 0, \quad \frac{\nu \lambda_{i+\frac{1}{2}}}{2} > 0, \quad \text{and} \quad \frac{\nu \lambda_{i-\frac{1}{2}}}{2} > 0. \quad (4.9)$$

Additionally, note that the coefficients in (4.7) sum to unity:

$$\left[1 - \frac{\nu}{2} (\lambda_{i+\frac{1}{2}} + \lambda_{i-\frac{1}{2}}) \right] + \left[\frac{\nu \lambda_{i+\frac{1}{2}}}{2} \right] + \left[\frac{\nu \lambda_{i-\frac{1}{2}}}{2} \right] = 1. \quad (4.10)$$

Now let C_α be any convex function of the conserved variables: $\underline{q} = (M_0, M_1, M_2, M_3, M_4)$. Then, applying the convex function to both sides of (4.7) we see that

$$\begin{aligned} C_\alpha(\underline{Q}_i^{n+1}) &\leq \left[1 - \frac{\nu}{2} (\lambda_{i+\frac{1}{2}} + \lambda_{i-\frac{1}{2}}) \right] C_\alpha(\underline{Q}_i^n) \\ &\quad + \left[\frac{\nu \lambda_{i+\frac{1}{2}}}{2} \right] C_\alpha(\underline{M}_i^+) + \left[\frac{\nu \lambda_{i-\frac{1}{2}}}{2} \right] C_\alpha(\underline{M}_i^-), \end{aligned} \quad (4.11)$$

which follows from the convexity assumption and from the conditions in (4.9) and (4.10).

Furthermore, we note that density, pressure, and modified kurtosis (ρ , p , and k) are all convex functions of $\underline{q} = (M_0, M_1, M_2, M_3, M_4)$; the density is trivially convex, while the pressure is convex if $\rho > 0$, and the modified kurtosis is convex if $\rho > 0$ and $p > 0$ (see definitions (1.8)). Therefore, in order to prove result (4.2), all we need to show is that

$$C_\alpha(\underline{M}_i^+) > 0 \quad \text{and} \quad C_\alpha(\underline{M}_i^-) > 0, \quad (4.12)$$

with C_α chosen as the density, pressure, and modified kurtosis:

$$\begin{aligned} C_\rho(\underline{q}) &:= q_1, & C_p(\underline{q}) &:= q_3 - \frac{q_2^2}{q_1}, \\ C_k(\underline{q}) &:= \frac{q_3^3 - 2q_2q_3q_4 + q_1q_4^2 + q_2^2q_5 - q_1q_3q_5}{q_2^2 - q_1q_3}. \end{aligned} \quad (4.13)$$

1. **Density:** We take $\alpha \equiv \rho$ and note that

$$C_\rho(\underline{Q} \pm \lambda^{-1} \underline{f}(\underline{Q})) = \frac{(\lambda \pm u)\rho}{\lambda}. \quad (4.14)$$

Positivity of (4.14) follows from the fact that the wave speed, λ , always exceeds the local fluid speed, $|u|$.

2. **Pressure:** We take $\alpha \equiv p$ and note that

$$C_p(\underline{Q} \pm \lambda^{-1} \underline{f}(\underline{Q})) = \frac{p\rho(\lambda \pm u)^2 + q\rho(u \pm \lambda) - p^2}{\lambda(\lambda \pm u)\rho}, \quad (4.15)$$

for which we note that the numerator is a quadratic polynomial in λ . The roots of this quadratic polynomial can easily be computed:

$$z_1 = \mp \left(u + \frac{q}{2p} \right) - \sqrt{\frac{p}{\rho} + \left(\frac{q}{2p} \right)^2}, \quad z_2 = \mp \left(u + \frac{q}{2p} \right) + \sqrt{\frac{p}{\rho} + \left(\frac{q}{2p} \right)^2}.$$

Positivity of (4.15) follows from the fact that $\lambda > \max\{z_1, z_2\}$ (i.e., λ is always to the right of the roots) and $p\rho > 0$ (i.e., the quadratic is concave up).

3. **Modified kurtosis:** We take $\alpha \equiv k$ and note that

$$C_k(\underline{Q} \pm \lambda^{-1} \underline{f}(\underline{Q})) = \left(\frac{k(\lambda \pm u)}{\lambda} \right) \left(\frac{p\rho(\lambda \pm u)^2 + q\rho(u \pm \lambda) - p^2 - k\rho}{p\rho(\lambda \pm u)^2 + q\rho(u \pm \lambda) - p^2} \right), \quad (4.16)$$

where the numerator of the second fraction is again a quadratic polynomial in λ . Showing that this quadratic is positive is sufficient to show that the whole expression is positive, since the remaining pieces are already positive due to the previously established positivity of (4.14) and (4.15). The roots of the quadratic are:

$$z_1 = \mp \left(u + \frac{q}{2p} \right) - \sqrt{\frac{k}{p} + \frac{p}{\rho} + \left(\frac{q}{2p} \right)^2}, \quad z_2 = \mp \left(u + \frac{q}{2p} \right) + \sqrt{\frac{k}{p} + \frac{p}{\rho} + \left(\frac{q}{2p} \right)^2}.$$

Positivity of (4.16) follows from the fact that $\lambda > \max\{z_1, z_2\}$ (i.e., λ is always to the right of the roots) and $p\rho > 0$ (i.e., the quadratic is concave up).

■

We have now shown that under an appropriate CFL condition, the first order method will maintain positivity from one time-step to the next. However, higher order methods will not automatically guarantee positivity; we address this issue in the subsequent subsections.

4.2 Limiter I: Positivity-at-points in the prediction step

The prediction step as described in (3.21) requires numerical quadrature in space-time in each Picard iteration. Furthermore, once the predicted solution has been computed, it will again be integrated in space-time in the correction step (i.e., see (3.24)–(3.27)). In order to guarantee that all of the numerical quadrature in both the prediction and correction steps only use positive values of density, pressure, and modified kurtosis, we introduce a prediction-step positivity limiter.

Let the 1D Gauss-Legendre points internal to each element, augmented by the element end-points (i.e., the location of the element faces), be defined as follows:

$$\mathbb{X}_{M_O} := \{-1, 1\} \cup \{\text{roots of the } M_O^{\text{th}} \text{ degree Legendre polynomial}\}, \quad (4.17)$$

where M_O is the desired order of accuracy. Note that \mathbb{X}_{M_O} contains a total of $M_O + 2$ points. We note that all of the quadrature in the prediction update (3.21) and correction update (3.24)–(3.27) only depends on the predicted solution at a small number of quadrature points, which are fully contained in the Cartesian product of \mathbb{X}_{M_O} with itself:

$$\mathbb{X}_{M_O}^2 := \mathbb{X}_{M_O} \otimes \mathbb{X}_{M_O}. \quad (4.18)$$

Therefore, $\mathbb{X}_{M_O}^2$ contains a total of $(M_O + 2)^2$ points. Our goal is thus to enforce positivity at all the space-time points $(\tau, \xi) \in \mathbb{X}_{M_O}^2$.

Following the strategy developed by Zhang and Shu [43] for the Runge-Kutta discontinuous Galerkin scheme, we apply the following procedure, which is applied element-by-element.

Step 1. On the current space-time element defined over

$$(t, x) \in [t^n, t^n + \Delta t] \times \left[x_i - \frac{\Delta x}{2}, x_i + \frac{\Delta x}{2} \right],$$

the solution is given by (3.17). Find the minimum density, pressure, and modified kurtosis of this solution over the points $(\tau, \xi) \in \mathbb{X}_{M_O}^2$:

$$\alpha_i^{(m)} := \min_{(\tau, \xi) \in \mathbb{X}_{M_O}^2} \left\{ \underline{\Psi}(\tau, \xi)^T \underline{W}_{i(:, m)}^{n+\frac{1}{2}} \right\}, \quad (4.19)$$

for $m = 1$ (density), $m = 3$ (pressure), and $m = 5$ (modified kurtosis).

Step 2. Rewrite the solution as

$$\underline{\alpha}^{\text{ST}} \left(t^n + \frac{\Delta t}{2}(1 + \tau), x_i + \frac{\Delta x}{2} \xi; \theta \right) := (1 - \theta) \underline{W}_{i(1,:)}^{n+\frac{1}{2}} + \theta \underline{\Psi}(\tau, \xi)^T \underline{W}_i^{n+\frac{1}{2}}, \quad (4.20)$$

where $\theta \in [0, 1]$, such that $\theta = 1$ recovers the original solution (3.17) and $\theta = 0$ results in reducing the entire solution on to its space-time average. We now choose the largest possible $\theta \in [0, 1]$ so that (4.20) is positive for components

$m = 1$ (density), 3 (pressure), 5 (modified kurtosis) at all the space-time points in $\mathbb{X}_{M_0}^2$. This achieved by taking

$$\theta = \min_{m \in \{1,3,5\}} \min \left\{ 1, \frac{W_{i(1,m)}^{n+\frac{1}{2}} - \varepsilon}{W_{i(1,m)}^{n+\frac{1}{2}} - \alpha_i^{(m)}} \right\}, \quad (4.21)$$

where $\varepsilon > 0$ is a preselected small constant (e.g., in this work we select $\varepsilon = 10^{-14}$).

4.3 Limiter II: Positivity-in-the-mean in the correction step

One of the key challenges in the correction step as described by (3.24)–(3.27) is to make sure that element averages of the density, pressure, and modified kurtosis remain positive at the end of the time-step: $\bar{\rho}_i^{n+1} > 0$, $\bar{p}_i^{n+1} > 0$, and $\bar{k}_i^{n+1} > 0$, where the bar over each variable refers to the element average. The prediction step limiter described in the previous subsection, §4.2, helps with this positivity-in-the-mean, but cannot guarantee it. Furthermore, without positivity-in-the-mean, we cannot achieve positivity of the higher-order polynomial inside the element (i.e., if the polynomial average is negative, a significant portion of the polynomial must be negative inside the element). In order to overcome this challenge we extend the approach developed by Moe et al. [31], which, for the element averages, blends the high-order update described by (3.24)–(3.27) with a first-order Rusanov scheme. We have already proved in Theorem 4.1 that the Rusanov scheme is guaranteed to preserve positivity.

We begin by defining the Rusanov [37] (aka local Lax-Friedrichs) update based on the element averages at $t = t^n$:

$$\underline{Q}_i^{\text{Rus}} := \underline{Q}_{i(1,:)}^n - \nu \left(\underline{\mathcal{F}}_{i+\frac{1}{2}}^{\text{Rus}} - \underline{\mathcal{F}}_{i-\frac{1}{2}}^{\text{Rus}} \right), \quad (4.22)$$

where $\nu = \Delta t / \Delta x$, the numerical flux is given by

$$\underline{\mathcal{F}}_{i-\frac{1}{2}}^{\text{Rus}} := \frac{1}{2} \left[\underline{f} \left(\underline{Q}_{i(1,:)}^n \right) + \underline{f} \left(\underline{Q}_{i-1(1,:)}^n \right) \right] - \frac{1}{2} |\lambda_{i-\frac{1}{2}}| \left(\underline{Q}_{i(1,:)}^n - \underline{Q}_{i-1(1,:)}^n \right), \quad (4.23)$$

and $|\lambda_{i-\frac{1}{2}}|$ is a local bound of the flux Jacobian spectral radius. Recall that $\underline{Q}_i^{\text{Rus}}$ is guaranteed to have positive density, pressure, and modified kurtosis under a time-step restriction (see Theorem 4.1).

Next we write the update for the element averages of the high-order method in terms of the low-order update (4.22):

$$\underline{Q}_{i(1,:)}^{n+1} = \underline{Q}_{i(1,:)}^{\text{Rus}} - \nu \left(\theta_{i+\frac{1}{2}} \underline{\Delta \mathcal{F}}_{i+\frac{1}{2}} - \theta_{i-\frac{1}{2}} \underline{\Delta \mathcal{F}}_{i-\frac{1}{2}} \right), \quad (4.24)$$

where the difference between the high and low order fluxes is given by

$$\underline{\Delta \mathcal{F}}_{i-\frac{1}{2}} := \underline{\mathcal{F}}_{i-\frac{1}{2}}^{n+\frac{1}{2}} - \underline{\mathcal{F}}_{i-\frac{1}{2}}^{\text{Rus}}, \quad (4.25)$$

and $\theta_{i+\frac{1}{2}} \in [0, 1]$ measures the amount of flux limiting, where $\theta_{i+\frac{1}{2}} = 0$ represents maximal limiting (i.e., no high-order flux contributions) and $\theta_{i+\frac{1}{2}} = 1$ represents no limiting (i.e., no low-order flux contributions).

The strategy for the positivity-in-the-mean limiter is then to find the maximum $\theta_{i+\frac{1}{2}} \in [0, 1]$ such that $\forall i$

$$C_\alpha \left(\underline{Q}_{i(1,:)}^{n+1} \right) > 0, \quad (4.26)$$

for $\alpha \equiv \rho$ (density), $\alpha \equiv p$ (pressure), and $\alpha \equiv k$ (modified kurtosis), as defined in (4.13). The strategy for achieving this is outlined below and is applied element-by-element. The process begins by initializing $\theta_{i+\frac{1}{2}} = 1 \forall i$.

Step 1: (density) Let $\nu = \Delta t / \Delta x$ and define

$$\Gamma := \frac{Q_{i(1)}^{\text{Rus}} - \varepsilon}{\nu}. \quad (4.27)$$

Set $\Lambda_{\text{left}} = \Lambda_{\text{right}} = 1$ (i.e., full high-order flux), but modify these if there is any potential for the density to decrease below zero.

Case 1. If $\Delta \mathcal{F}_{i-\frac{1}{2}}(1) < 0$ and $\Delta \mathcal{F}_{i+\frac{1}{2}}(1) < 0$, then

$$\Lambda_{\text{left}} = \Lambda_{\text{right}} = \min \left\{ 1, \frac{\Gamma}{\left| \Delta \mathcal{F}_{i-\frac{1}{2}}(1) \right| + \left| \Delta \mathcal{F}_{i+\frac{1}{2}}(1) \right|} \right\}. \quad (4.28)$$

Case 2. If $\Delta \mathcal{F}_{i-\frac{1}{2}}(1) < 0$ and $\Delta \mathcal{F}_{i+\frac{1}{2}}(1) > 0$ then

$$\Lambda_{\text{left}} = \min \left\{ 1, \frac{\Gamma}{\left| \Delta \mathcal{F}_{i-\frac{1}{2}}(1) \right|} \right\}. \quad (4.29)$$

Case 3. If $\Delta \mathcal{F}_{i+\frac{1}{2}}(1) < 0$ and $\Delta \mathcal{F}_{i-\frac{1}{2}}(1) > 0$ then

$$\Lambda_{\text{right}} = \min \left\{ 1, \frac{\Gamma}{\left| \Delta \mathcal{F}_{i+\frac{1}{2}}(1) \right|} \right\}. \quad (4.30)$$

Step 2: (pressure) Compute the Rusanov pressure (which is guaranteed to be positive):

$$p^{\text{Rus}} := C_p \left(\underline{Q}_i^{\text{Rus}} \right). \quad (4.31)$$

Set $\mu_{11} = \mu_{10} = \mu_{01} = 1$, but modify these if there is any potential for the pressure to decrease below zero.

Part 2A. Set

$$\underline{Q}^\star = \underline{Q}_{i(1,:)}^n - \nu \left(\Lambda_{\text{right}} \underline{\mathcal{F}}_{i+\frac{1}{2}}^{n+\frac{1}{2}} - \Lambda_{\text{left}} \underline{\mathcal{F}}_{i-\frac{1}{2}}^{n+\frac{1}{2}} \right), \quad p^\star = C_p \left(\underline{Q}^\star \right). \quad (4.32)$$

If $p^\star < \varepsilon$, then we set $\mu_{11} = (p^{\text{Rus}} - \varepsilon) / (p^{\text{Rus}} - p^\star)$.

Part 2B. Set

$$\underline{Q}^\star = \underline{Q}_{i(1,:)}^n + \nu \Lambda_{\text{left}} \underline{\mathcal{F}}_{i-\frac{1}{2}}^{n+\frac{1}{2}}, \quad p^\star = C_p(\underline{Q}^\star). \quad (4.33)$$

If $p^\star < \varepsilon$, then $\mu_{10} = (p^{\text{Rus}} - \varepsilon) / (p^{\text{Rus}} - p^\star)$.

Part 2C. Set

$$\underline{Q}^\star = \underline{Q}_{i(1,:)}^n - \nu \Lambda_{\text{right}} \underline{\mathcal{F}}_{i+\frac{1}{2}}^{n+\frac{1}{2}}, \quad p^\star = C_p(\underline{Q}^\star). \quad (4.34)$$

If $p^\star < \varepsilon$, then $\mu_{01} = (p^{\text{Rus}} - \varepsilon) / (p^{\text{Rus}} - p^\star)$.

Part 2D. Set

$$\mu = \min\{\mu_{11}, \mu_{10}, \mu_{01}\}, \quad \Lambda_{\text{left}} \leftarrow \mu \Lambda_{\text{left}}, \quad \Lambda_{\text{right}} \leftarrow \mu \Lambda_{\text{right}}. \quad (4.35)$$

Step 3: (modified kurtosis) Compute the Rusanov modified kurtosis (which is guaranteed to be positive):

$$k^{\text{Rus}} := C_k(\underline{Q}_i^{\text{Rus}}). \quad (4.36)$$

Set $\mu_{11} = \mu_{10} = \mu_{01} = 1$, but modify these if there is any potential for the pressure to decrease below zero.

Part 3A. Set

$$\underline{Q}^\star = \underline{Q}_{i(1,:)}^n - \nu \left(\Lambda_{\text{right}} \underline{\mathcal{F}}_{i+\frac{1}{2}}^{n+\frac{1}{2}} - \Lambda_{\text{left}} \underline{\mathcal{F}}_{i-\frac{1}{2}}^{n+\frac{1}{2}} \right), \quad k^\star = C_k(\underline{Q}^\star). \quad (4.37)$$

If $k^\star < \varepsilon$, then we set $\mu_{11} = (k^{\text{Rus}} - \varepsilon) / (k^{\text{Rus}} - k^\star)$.

Part 3B. Set

$$\underline{Q}^\star = \underline{Q}_{i(1,:)}^n + \nu \Lambda_{\text{left}} \underline{\mathcal{F}}_{i-\frac{1}{2}}^{n+\frac{1}{2}}, \quad k^\star = C_k(\underline{Q}^\star). \quad (4.38)$$

If $k^\star < \varepsilon$, then $\mu_{10} = (k^{\text{Rus}} - \varepsilon) / (k^{\text{Rus}} - k^\star)$.

Part 3C. Set

$$\underline{Q}^\star = \underline{Q}_{i(1,:)}^n - \nu \Lambda_{\text{right}} \underline{\mathcal{F}}_{i+\frac{1}{2}}^{n+\frac{1}{2}}, \quad k^\star = C_k(\underline{Q}^\star). \quad (4.39)$$

If $k^\star < \varepsilon$, then $\mu_{01} = (p^{\text{Rus}} - \varepsilon) / (k^{\text{Rus}} - k^\star)$.

Part 3D. Set

$$\mu = \min\{\mu_{11}, \mu_{10}, \mu_{01}\}, \quad \Lambda_{\text{left}} \leftarrow \mu \Lambda_{\text{left}}, \quad \Lambda_{\text{right}} \leftarrow \mu \Lambda_{\text{right}}. \quad (4.40)$$

Step 4: Set

$$\theta_{i-\frac{1}{2}} \leftarrow \min\{\theta_{i-\frac{1}{2}}, \Lambda_{\text{left}}\} \quad \text{and} \quad \theta_{i+\frac{1}{2}} \leftarrow \min\{\theta_{i+\frac{1}{2}}, \Lambda_{\text{right}}\}. \quad (4.41)$$

In all of the above formulas, we select in this work: $\varepsilon = 10^{-14}$.

4.4 Limiter III: Positivity-at-points in the correction step

Once we have ensured that the element averages are positive, we then look to enforce positivity of the corrected solution at spatial quadrature points: $\xi \in \mathbb{X}_{M_0}$ as defined by (4.17). Following the ideas developed by Zhang and Shu [43] for the Runge-Kutta discontinuous Galerkin scheme, we aim to find the maximum $\theta \in [0, 1]$ such that

$$\underline{q}^h \left(t^{n+1}, x_i + \frac{\Delta x}{2} \xi; \theta \right) := (1 - \theta) \underline{Q}_{i(1,:)}^{n+1} + \theta \underline{\Phi}(\xi)^T \underline{Q}_i^{n+1} \quad (4.42)$$

is positive at all points $\xi \in \mathbb{X}_{M_0}$ for every space element \mathcal{T}_i . Just as in the prediction step limiter from §4.2, $\theta = 0$ means that the solution is limited fully down to its element average, while $\theta = 1$ means that no limiting is needed and the full high-order approximation can be used. We apply the following procedure element-by-element.

Step 1. On the current element defined over

$$x \in \left[x_i - \frac{\Delta x}{2}, x_i + \frac{\Delta x}{2} \right],$$

the solution is given by (3.11). Find the minimum density $\forall \xi \in \mathbb{X}_{M_0}$ (see (4.17)) and compute the corresponding damping parameter (θ):

$$\rho_i^{\min} := \min_{\xi \in \mathbb{X}_{M_0}} \left\{ \underline{\Phi}(\xi)^T \underline{Q}_{i(:,1)}^{n+1} \right\}, \quad \theta = \min \left\{ 1, \frac{Q_{i(1,1)}^{n+1} - \varepsilon}{Q_{i(1,1)}^{n+1} - \rho_i^{\min}} \right\}. \quad (4.43)$$

Finally, rescale the higher-order coefficients using the above calculated damping parameter (θ):

$$\underline{Q}_{i(:,\ell)}^{n+1} \leftarrow \theta \underline{Q}_{i(:,\ell)}^{n+1} \quad \forall \ell = 2, \dots, M_C. \quad (4.44)$$

Step 2. Now that the density is positive $\forall \xi \in \mathbb{X}_{M_0}$, we repeat **Step 1** for the pressure. That is, we find the average pressure and the minimum pressure $\forall \xi \in \mathbb{X}_{M_0}$:

$$\bar{P}_i := C_p \left(\underline{Q}_{i(1,:)}^{n+1} \right), \quad p_i^{\min} := \min_{\xi \in \mathbb{X}_{M_0}} \left\{ C_p \left(\underline{\Phi}(\xi)^T \underline{Q}_i^{n+1} \right) \right\}, \quad (4.45)$$

where $C_p(\underline{q})$ is defined in (4.13). From here we compute the corresponding damping parameter and rescale the higher-order coefficients:

$$\theta = \min \left\{ 1, \frac{\bar{P}_i - \varepsilon}{\bar{P}_i - p_i^{\min}} \right\}, \quad \underline{Q}_{i(:,\ell)}^{n+1} \leftarrow \theta \underline{Q}_{i(:,\ell)}^{n+1} \quad \forall \ell = 2, \dots, M_C. \quad (4.46)$$

Step 3. Now that both density and pressure are positive $\forall \xi \in \mathbb{X}_{M_0}$, we repeat **Step 2** for the modified kurtosis. That is, we find the average modified kurtosis and the minimum modified kurtosis $\forall \xi \in \mathbb{X}_{M_0}$:

$$\bar{K}_i := C_k \left(\underline{Q}_{i(1,:)}^{n+1} \right), \quad k_i^{\min} := \min_{\xi \in \mathbb{X}_{M_0}} \left\{ C_k \left(\underline{\Phi}(\xi)^T \underline{Q}_i^{n+1} \right) \right\}, \quad (4.47)$$

where $C_k(\underline{q})$ is defined in (4.13). From here we compute the corresponding damping parameter and rescale the higher-order coefficients:

$$\theta = \min \left\{ 1, \frac{\bar{K}_i - \varepsilon}{\bar{K}_i - k_i^{\min}} \right\}, \quad \underline{Q}_{i(:,\ell)}^{n+1} \leftarrow \theta \underline{Q}_{i(:,\ell)}^{n+1} \quad \forall \ell = 2, \dots, M_C. \quad (4.48)$$

In all the formulas presented above we use $\varepsilon = 10^{-14}$.

4.5 Limiter IV: Unphysical oscillation limiter

The previously described limiters guarantee positivity for ρ , p , and k , but there still may be unphysical oscillations near shocks, rarefactions, or large gradients. To eliminate these oscillations, we augment the method with one more limiter: a variant of the strategy developed in Moe et al. [30]. This limiter is applied once per time step, and is able to remove unphysical oscillations without overly diffusing the numerical solution. We apply the following procedure.

Step 1. Loop over each element \mathcal{T}_i and compute the minimum and maximum values of all primitive variables: $w^\ell \in \{\rho, u, p, q, k\}$:

$$w_{M_i}^\ell := \max_{\xi \in \mathbb{X}_{M_O}} \left\{ w^\ell \left(\underline{q}^h(\xi) \right) \Big|_{\mathcal{T}_i} \right\}, \quad w_{m_i}^\ell := \min_{\xi \in \mathbb{X}_{M_O}} \left\{ w^\ell \left(\underline{q}^h(\xi) \right) \Big|_{\mathcal{T}_i} \right\}, \quad (4.49)$$

for all $\ell = 1, 2, 3, 4, 5$.

Step 2. Compute upper and lower bounds over all neighborhoods, $N_{\mathcal{T}_i} := \{\mathcal{T}_{i-1}, \mathcal{T}_i, \mathcal{T}_{i+1}\}$:

$$M_i^\ell = \max \left\{ \bar{w}_i^\ell + \alpha, \max_{j \in N_{\mathcal{T}_i}} \left\{ w_{M_j}^\ell \right\} \right\}, \quad m_i^\ell = \min \left\{ \bar{w}_i^\ell - \alpha, \min_{j \in N_{\mathcal{T}_i}} \left\{ w_{m_j}^\ell \right\} \right\}, \quad (4.50)$$

where \bar{w}_i^ℓ are the element averages of each of the primitive variables, and $\alpha = 5h^{1.5}$ is used to offset these averages to recover high-order accuracy for smooth solutions in the limit $h \rightarrow 0$ (see Moe et al. [30] for more details).

Step 3. On each element \mathcal{T}_i , compute the largest damping parameters between $[0, 1]$ that guarantee that the high-order solution in \mathcal{T}_i does not violate the maximum and minimum bounds defined by (4.50):

$$\theta = \min \left\{ 1, \mu \cdot \min_{\ell} \left\{ \frac{M_i^\ell - \bar{w}_i^\ell}{w_{M_i}^\ell - \bar{w}_i^\ell} \right\}, \mu \cdot \min_{\ell} \left\{ \frac{m_i^\ell - \bar{w}_i^\ell}{w_{m_i}^\ell - \bar{w}_i^\ell} \right\} \right\}, \quad (4.51)$$

where the factor $\mu = 10/11$ is introduced to slightly increase the aggressiveness of the limiter (again, see Moe et al. [30] for more details).

Step 4. On each element \mathcal{T}_i , limit the conserved variables:

$$\underline{Q}_{i(:,\ell)}^{n+1} \leftarrow \theta \underline{Q}_{i(:,\ell)}^{n+1} \quad \forall \ell = 2, \dots, M_C. \quad (4.52)$$

5 Numerical examples

In this section we apply the proposed scheme and the corresponding limiters to several test cases. In §5.1 we verify the claimed orders of accuracy on a smooth exact solution. In §5.2 and §5.3 we apply the scheme to *shock tube* initial data. These results clearly demonstrate the ability of the non-oscillatory limiter to control unphysical oscillations. Finally, in §5.4 we fully validate the positivity limiters by applying the scheme to piecewise constant initial data that lead to the formation of a vacuum. This example demonstrates the ability of the positivity limiters to prevent negative states in density, pressure, and modified kurtosis, both on the element average, as well as on the solution values internal to the element. In all the cases presented in §5.2, §5.3, and §5.4, we compare the high-order scheme against a highly-resolved first-order Rusanov scheme that is guaranteed to be positivity-preserving without the need for any limiters.

5.1 Smooth solution convergence test

Consider the following exact solution to the 1D HyQMOM system (2.27)–(2.28) with periodic boundary conditions on $x \in [-1, 1]$:

$$\begin{aligned} \rho(t, x) &= 2 + \sin(2\pi(x - t)), \\ u(t, x) &= 1, \quad p(t, x) = 2, \quad q(t, x) = 4, \quad k(t, x) = 8 - 4[\rho(t, x)]^{-1}. \end{aligned} \quad (5.1)$$

The numerical solution is computed with grid resolutions of

$$M_{\text{elem}} = 10 \times 2^k, \quad \text{for } k = 0, 1, 2, 3, 4, 5, \quad (5.2)$$

up to a final time of $t = 1$. We verify the order of accuracy for the schemes with orders of accuracy $M_O = 2, 3, 4$.

The errors we report are based on the following error measure:

$$\sum_{\ell=1}^{M_{\text{eqn}}} \frac{\|f_\ell - g_\ell\|_{L^2[-1,1]}}{\|g_\ell\|_{L^2[-1,1]}} = \sum_{\ell=1}^{M_{\text{eqn}}} \sqrt{\frac{\int_{-1}^1 |f_\ell(x) - g_\ell(x)|^2 dx}{\int_{-1}^1 |g_\ell(x)|^2 dx}}, \quad (5.3)$$

where $f(x) : [-1, 1] \mapsto \mathbb{R}^{M_{\text{eqn}}}$ is the approximate solution and $g(x) : [-1, 1] \mapsto \mathbb{R}^{M_{\text{eqn}}}$ is the exact solution. In practice, however, we replace the exact solution with a piecewise Legendre polynomial approximation of degree $M_O + 1$ on the computational mesh. Repeated use of the orthonormality of the Legendre basis functions yields the following (approximate) relative error on a mesh with N elements and a numerical method of order M_O :

$$e_N := \sum_{\ell=1}^{M_{\text{eqn}}} \sqrt{\frac{\sum_{i=1}^N \left\{ \sum_{k=1}^{M_C} \left(Q_{i(k,\ell)} - Q_{i(k,\ell)}^* \right)^2 + \left(Q_{i(M_C+1,\ell)}^* \right)^2 \right\}}{\sum_{i=1}^N \sum_{k=1}^{M_C+1} \left(Q_{i(k,\ell)}^* \right)^2}}, \quad (5.4)$$

N	$M_O = 1$	Eq. (5.6)	$M_O = 2$	Eq. (5.6)	$M_O = 3$	Eq. (5.6)
10	1.015e-01	—	1.024e-02	—	4.945e-03	—
20	1.488e-02	2.770	2.144e-03	2.256	4.656e-04	3.409
40	1.647e-03	3.175	3.930e-04	2.448	5.051e-06	6.526
80	1.983e-04	3.055	5.973e-05	2.718	1.370e-07	5.204
160	4.643e-05	2.094	8.005e-06	2.899	8.435e-09	4.022
320	1.186e-05	1.968	1.025e-06	2.965	5.147e-10	4.035

Table 5.1 (§5.1: smooth solution convergence test) Relative L^2 errors for the HyQMOM equations with variable density, constant fluid velocity, pressure, heat flux, and fourth primitive moment, and periodic boundary conditions.

where Q and Q^* are the Legendre coefficients of the numerical and exact solutions at the final time, respectively. The exact solution coefficients are computed using Gaussian quadrature with 20 quadrature points per element:

$$\underline{Q}_{i(k,:)}^* := \frac{1}{2} \sum_{a=1}^{20} \omega_a^* \phi_k(\mu_a^*) \underline{q}^* \left(t = 1, x_i + \frac{\Delta x}{2} \mu_a^* \right), \quad (5.5)$$

where ω_a^* and μ_a^* for $a = 1, \dots, 20$ are the weights and abscissas of the 20 point quadrature rule, and \underline{q}^* is the exact solution. Gaussian quadrature rules have been tabulated in many books and websites; we obtained our data from [23].

The errors as defined by (5.4), as well as the base-2 logarithms of the ratio of consecutive errors,

$$\log_2 \left(\frac{e_{N/2}}{e_N} \right) \approx \log_2 \left(\frac{(N/2)^{-M_O}}{N^{-M_O}} \right) = \log_2 \left(2^{M_O} \right) = M_O, \quad (5.6)$$

are shown in Table 5.1.

5.2 Shock tube problem #1

Consider the Riemann problem for (2.27)–(2.29) with the following initial data at $t = 0$:

$$(\rho, u, p, q, k)(t = 0, x) = \begin{cases} (1.5, -0.5, 1.5, 1.0, 2.3\bar{3}) & x < 0, \\ (1.0, -0.5, 1.0, 0.5, 1.75) & x > 0, \end{cases} \quad (5.7)$$

on $x \in [-1.2, 1.2]$ with extrapolation boundary conditions.

Shown in Figure 5.1 are results from a simulation run with two distinct methods: (1) the $M_O = 4$ scheme with 200 elements and full limiters (shown as blue dots) and (2) the first-order Rusanov scheme with 20,000 elements (shown as a solid red line). For the $M_O = 4$ scheme we are plotting 4 points-per-element in order to show the intra-element solution structure. The panels show the primitive variables: (a) density:

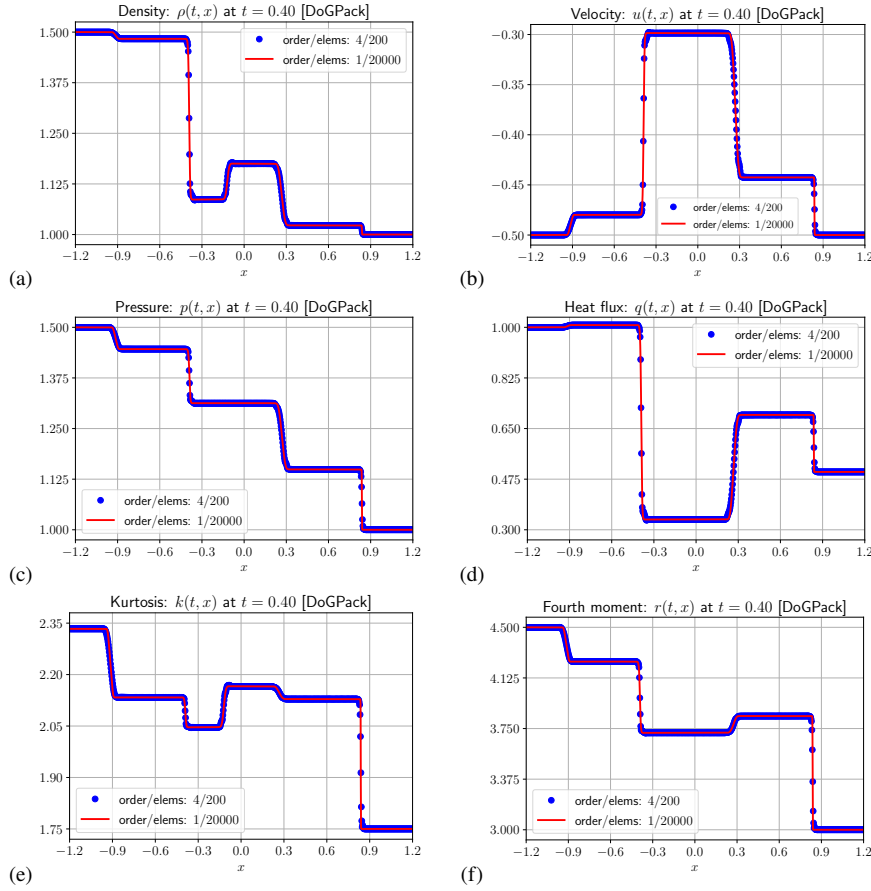


Fig. 5.1 (§5.2: shock tube problem #1) Numerical solution of shock tube problem #1 on $x \in [-1.2, 1.2]$ with initial conditions given by (5.7). Shown are results from a simulation run with two distinct methods: (1) the $M_O = 4$ scheme with 200 elements and full limiters (shown as blue dots) and (2) the first-order Rusanov scheme with 20,000 elements (shown as a solid red line). For the $M_O = 4$ scheme we are plotting 4 points-per-element in order to show the intra-element solution structure. The panels show the primitive variables: (a) density: $\rho(t, x)$, (b) macroscopic velocity: $u(t, x)$, (c) pressure: $p(t, x)$, (d) heat flux: $q(t, x)$, (e) modified kurtosis: $k(t, x)$, and (f) primitive fourth-moment: $r(t, x)$.

$\rho(t, x)$, (b) macroscopic velocity: $u(t, x)$, (c) pressure: $p(t, x)$, (d) heat flux: $q(t, x)$, (e) modified kurtosis: $k(t, x)$, and (f) primitive fourth-moment: $r(t, x)$.

These results clearly demonstrate the ability of the non-oscillatory limiters to adequately control unphysical oscillations and produce accurate solutions.

5.3 Shock tube problem #2

Consider the Riemann problem for (2.27)–(2.29) with the following initial data at $t = 0$:

$$(\rho, u, p, q, k)(t = 0, x) = \begin{cases} (1.0, -0.7, 1.5, 1.5, 1.75) & x < 0, \\ (0.5, -0.9, 1.0, 1.0, 1.0) & x > 0, \end{cases} \quad (5.8)$$

on $x \in [-1.2, 1.2]$ with extrapolation boundary conditions.

Shown in Figure 5.2 are results from a simulation run with two distinct methods: (1) the $M_O = 4$ scheme with 200 elements and full limiters (shown as blue dots) and (2) the first-order Rusanov scheme with 20,000 elements (shown as a solid red line). For the $M_O = 4$ scheme we are plotting 4 points-per-element in order to show the intra-element solution structure. The panels show the primitive variables: (a) density: $\rho(t, x)$, (b) macroscopic velocity: $u(t, x)$, (c) pressure: $p(t, x)$, (d) heat flux: $q(t, x)$, (e) modified kurtosis: $k(t, x)$, and (f) primitive fourth-moment: $r(t, x)$.

Again, just as in the previous example, these results clearly demonstrate the ability of the non-oscillatory limiters to adequately control unphysical oscillations and produce accurate solutions.

5.4 Double rarefaction vacuum problem

In the final example, we solve a vacuum problem where the right and left initial velocities are large and opposite, creating a vacuum state in the center of the solution domain. The initial states are

$$(\rho, u, p, q, k)(t = 0, x) = \begin{cases} (1.0, -2.0, 1.0, 0.0, 2.0) & x < 0, \\ (1.0, +2.0, 1.0, 0.0, 2.0) & x > 0. \end{cases} \quad (5.9)$$

The computational domain is $x \in [-1.2, 1.2]$ with extrapolation boundary conditions.

Shown in Figure 5.3 are results from a simulation run with two distinct methods: (1) the $M_O = 4$ scheme with 200 elements and full limiters (shown as blue dots) and (2) the first-order Rusanov scheme with 20,000 elements (shown as a solid red line). For the $M_O = 4$ scheme we are plotting 4 points-per-element in order to show the intra-element solution structure. The panels show the primitive variables: (a) density: $\rho(t, x)$, (b) macroscopic velocity: $u(t, x)$, (c) pressure: $p(t, x)$, (d) heat flux: $q(t, x)$, (e) modified kurtosis: $k(t, x)$, and (f) primitive fourth-moment: $r(t, x)$.

We comment on two important findings from this simulation. First, this example demonstrates the ability of the positivity limiters to prevent negative states in density, pressure, and modified kurtosis, both on the element average, as well as the solution values internal to the element. Second, while the simulation results from the $M_O = 4$ scheme with 200 elements does show some differences in the vacuum region with the highly resolved Rusanov solution, especially in the density plot shown in Figure 5.3(a), the solution still remains qualitatively correct. We can investigate this further by increasing the grid resolution; in Figure 5.4 we show the density plots at different grid resolutions: (a) $N = 200$, (b) $N = 400$, (c) $N = 800$, and (d) $N = 1600$. These results verify that the differences between the $M_O = 4$ scheme and the highly resolved Rusanov scheme disappear at higher resolutions.

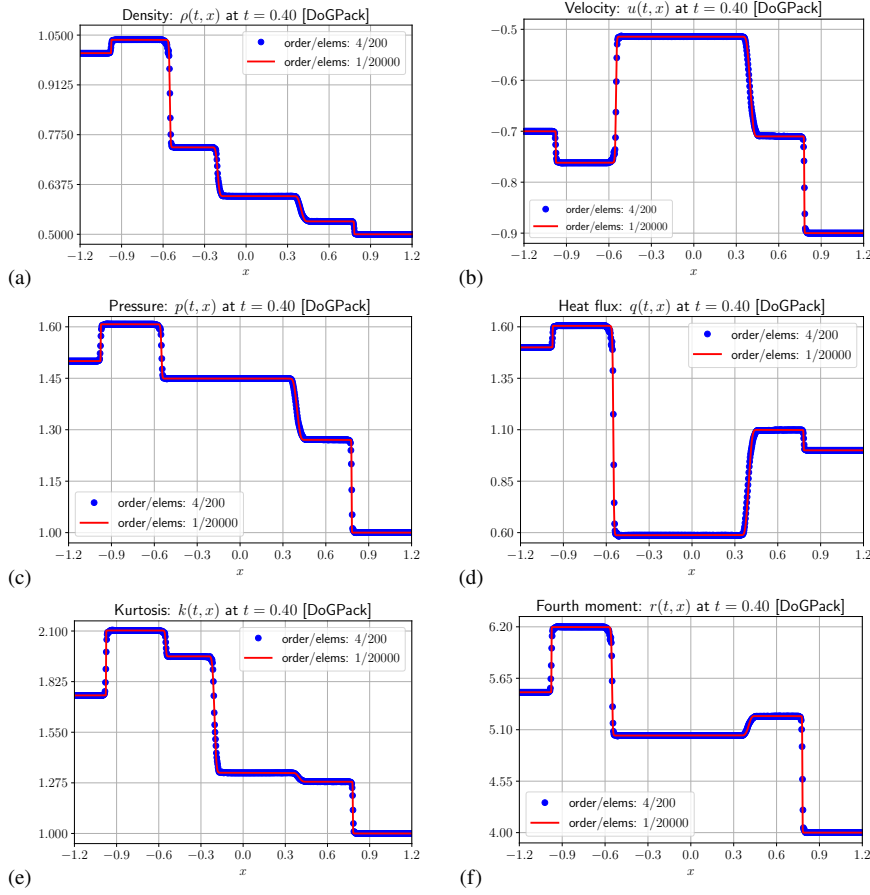


Fig. 5.2 (§5.3: shock tube problem #2) Numerical solution of shock tube problem #2 on $x \in [-1.2, 1.2]$ with initial conditions given by (5.8). Shown are results from a simulation run with two distinct methods: (1) the $M_O = 4$ scheme with 200 elements and full limiters (shown as blue dots) and (2) the first-order Rusanov scheme with 20,000 elements (shown as a solid red line). For the $M_O = 4$ scheme we are plotting 4 points-per-element in order to show the intra-element solution structure. The panels show the primitive variables: (a) density: $\rho(t, x)$, (b) macroscopic velocity: $u(t, x)$, (c) pressure: $p(t, x)$, (d) heat flux: $q(t, x)$, (e) modified kurtosis: $k(t, x)$, and (f) primitive fourth-moment: $r(t, x)$.

6 Conclusions

In this work we considered a particular moment closure called HyQMOM (the hyperbolic quadrature-based method of moments), which was originally introduced by Fox, Laurent, Vie [17], and further studied by Johnson [21] and Wiersma [42]. Quadrature-based method of moments (QMOM), including the HyQMOM variant, are a promising class of approximation techniques for reducing kinetic equations to fluid equations that are valid beyond thermodynamic equilibrium. In particular, the goal of the present work was to develop high-order discontinuous Galerkin schemes

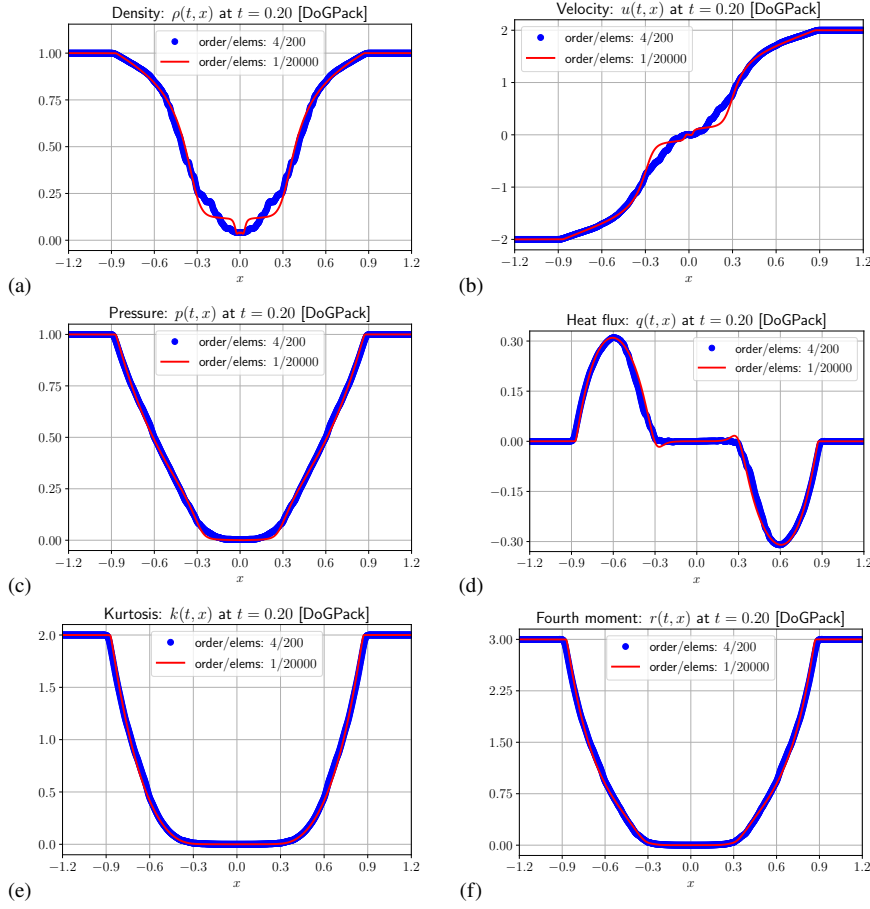


Fig. 5.3 (§5.4: double rarefaction vacuum problem) Numerical solution of the double rarefaction vacuum problem on $x \in [-1.2, 1.2]$ with initial conditions given by (5.9). Shown are results from a simulation run with two distinct methods: (1) the $M_O = 4$ scheme with 200 elements and full limiters (shown as blue dots) and (2) the first-order Rusanov scheme with 20,000 elements (shown as a solid red line). For the $M_O = 4$ scheme we are plotting 4 points-per-element in order to show the intra-element solution structure. The panels show the primitive variables: (a) density: $\rho(t, x)$, (b) macroscopic velocity: $u(t, x)$, (c) pressure: $p(t, x)$, (d) heat flux: $q(t, x)$, (e) modified kurtosis: $k(t, x)$, and (f) primitive fourth-moment: $r(t, x)$.

and corresponding limiters that control both unphysical oscillations and eliminate positivity violations.

The numerical scheme developed is based on the Lax-Wendroff discontinuous Galerkin scheme introduced by Qiu, Dumbser, and Shu [35], with the predictor-corrector interpretation developed by Gassner et al. [18], and further refinements developed by Felton et al. [13]. The resulting numerical method is performed in two phases at each time step.

Prediction step. In this phase, the equation and numerical solution are written in the primitive variables. In the space-time DG approximation which is applied on each

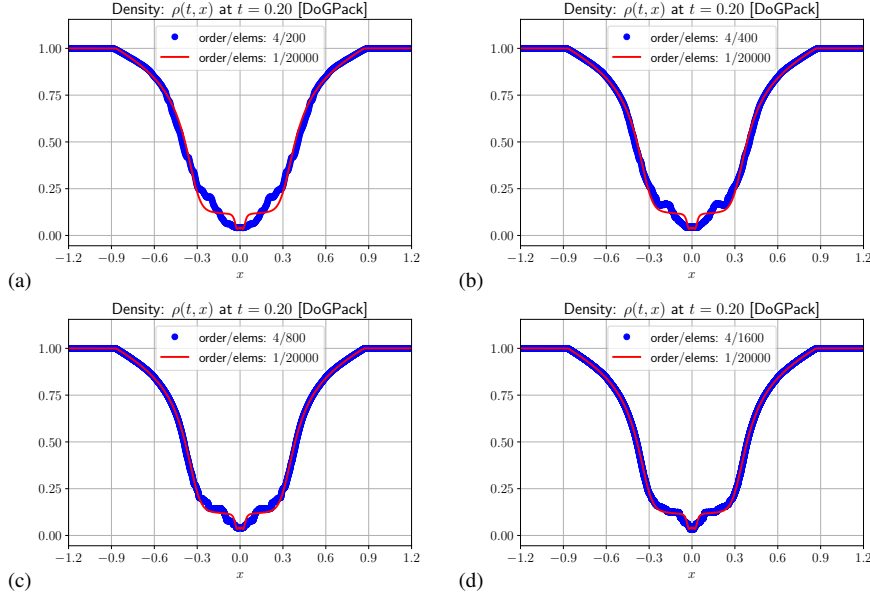


Fig. 5.4 (§5.4: double rarefaction vacuum problem) Numerical solution of the double rarefaction vacuum problem on $x \in [-1.2, 1.2]$ with initial conditions given by (5.9). Shown are the densities at various grid resolutions: (a) $N = 200$, (b) $N = 400$, (c) $N = 800$, and (d) $N = 1600$. In each panel we compare the $M_O = 4$ scheme with full limiters (shown as blue dots) with the first-order Rusanov scheme with 20,000 elements (shown as a solid red line).

element, integration-by-parts is only performed on the time variable. The result is a system of nonlinear equations that are local on each element. These equations are solved using a Picard iteration, which provides a sufficiently accurate solution after $M_O - 1$ iterations, where M_O is the order of accuracy of the method.

Correction step. The correction step is a forward Euler-like step which is applied to advance to the new time, $t = t^n + \Delta t$, where $t = t^n$ is the current time. This step is based on a DG scheme with integration-by-parts in the spatial variable and time integration of the predicted solution. The equation and numerical solution are written in the conservative variables.

In order to guarantee positivity and achieve solutions without unphysical oscillations, several limiters were applied to the scheme.

Limiter I: Prediction step positivity limiter. This limiter is completely local and minimally damps high-order corrections to the primitive variables to get pointwise positivity of the predicted density, pressure, and modified kurtosis on all space-time quadrature points (Gauss-Legendre + edges). The limiter is applied one time after each Picard iteration, meaning it is applied a total of $M_O - 1$ times per time step.

Limiter II: Correction step positivity limiter on cell average. This limiter is applied once per time step and blends high order numerical fluxes with positivity

preserving low order fluxes in such a way to preserve the positivity of the corrected element averages of density, pressure, and modified kurtosis. This limiter is applied once per time step.

Limiter III: Correction step positivity limiter on quadrature points. This limiter is similar to Limiter I, and involves minimally damping the high order corrections to preserve the positivity of the corrected density, pressure, and modified kurtosis, on all spatial quadrature points (Gauss-Legendre + edges). This limiter is applied once per time step at the end of the step.

Limiter IV: Oscillation Limiter. This limiter damps the solution if the primitive solution variables on the current element significantly exceed the primitive solution variables on neighboring elements. This limiter is applied once time per time step at the end of the time step.

The proposed high-order method and the limiting strategy was tested on both a smooth problem as well as on Riemann problems. The smooth solution was used to perform convergence tests that demonstrated the expected orders of accuracy. The Riemann data tests clearly showed that the limiters were successful in damping unphysical oscillations without adversely diffusing the solution, and that they were able to preserve the positivity of the relevant variables.

A Appendix

Lemma A.1 (Hermite interpolation) Consider the Hermite interpolation problem of interpolating the function $f(v) = v^{2N}$ with a polynomial of degree $2N-1$:

$$P_{2N-1}(v) = a_0 + a_1 v + a_2 v^2 + \dots + a_{2N-1} v^{2N-1} = \sum_{k=0}^{2N-1} a_k v^k, \quad (\text{A.1})$$

with interpolating conditions for $k = 0, 1, \dots, N$:

$$P_{2N-1}(\mu_k) = f(\mu_k) = \mu_k^{2N} \quad \text{and} \quad P'_{2N-1}(\mu_k) = f'(\mu_k) = 2N \mu_k^{2N-1}. \quad (\text{A.2})$$

Applying these conditions yields the following formula for the polynomial coefficients:

$$\begin{bmatrix} a_0 \\ \vdots \\ a_{N-1} \\ a_N \\ \vdots \\ a_{2N-1} \end{bmatrix} = \begin{bmatrix} 1 & \mu_1 & \mu_1^2 & \mu_1^3 & \dots & \mu_1^{2N-1} \\ \vdots & \vdots & \vdots & & & \vdots \\ 1 & \mu_N & \mu_N^2 & \mu_N^3 & \dots & \mu_N^{2N-1} \\ 0 & 1 & 2\mu_1 & 3\mu_1^2 & \dots & (2N-1)\mu_1^{2N-2} \\ \vdots & \vdots & \vdots & \vdots & & \vdots \\ 0 & 1 & 2\mu_N & 3\mu_N^2 & \dots & (2N-1)\mu_N^{2N-2} \end{bmatrix}^{-1} \begin{bmatrix} \mu_1^{2N} \\ \vdots \\ \mu_N^{2N} \\ 2N\mu_1^{2N-1} \\ \vdots \\ 2N\mu_N^{2N-1} \end{bmatrix}. \quad (\text{A.3})$$

Proof The claimed result follows directly from applying the interpolating conditions to the polynomial $P_{2N-1}(v)$. ■

Lemma A.2 (Moment gradient operator I) Let $f(\underline{\omega}, \underline{\mu}) : \mathbb{R}^N \times \mathbb{R}^N \mapsto \mathbb{R}$ be a continuously differentiable function. The gradient of f with respect to the moments, $\underline{\mathbf{M}} = (\mathbf{M}_0, \mathbf{M}_1, \dots, \mathbf{M}_{2N-1})$, is given by

$$\nabla_{\underline{\mathbf{M}}} f(\underline{\omega}, \underline{\mu}) = \underline{\mathbf{B}}^{-1} \nabla_{(\underline{\omega}, \underline{\mu})} f(\underline{\omega}, \underline{\mu}), \quad (\text{A.4})$$

where

$$\nabla_{\underline{M}} := \left(\frac{\partial}{\partial M_0}, \frac{\partial}{\partial M_1}, \dots, \frac{\partial}{\partial M_{2N-1}} \right), \quad (\text{A.5})$$

$$\nabla_{(\underline{\omega}, \underline{\mu})} := \left(\frac{\partial}{\partial \omega_1}, \dots, \frac{\partial}{\partial \omega_N}, \frac{\partial}{\partial \mu_1}, \dots, \frac{\partial}{\partial \mu_N} \right), \quad (\text{A.6})$$

$$\underline{B} := \frac{\partial \underline{M}}{\partial (\underline{\omega}, \underline{\mu})} = \begin{bmatrix} 1 & \mu_1 & \mu_1^2 & \cdots & \mu_1^{2N-1} \\ \vdots & \vdots & \vdots & & \vdots \\ 1 & \mu_N & \mu_N^2 & \cdots & \mu_N^{2N-1} \\ 0 & \omega_1 & 2\omega_1\mu_1 & \cdots & (2N-1)\omega_1\mu_1^{2N-2} \\ \vdots & \vdots & \vdots & & \vdots \\ 0 & \omega_N & 2\omega_N\mu_N & \cdots & (2N-1)\omega_N\mu_N^{2N-2} \end{bmatrix}. \quad (\text{A.7})$$

Proof The results follows directly from the chain rule applied to the definition of the moments:

$$M_p = \sum_{k=1}^N \omega_k \mu_k^p \quad \text{for } p = 0, 1, \dots, 2N-1. \quad (\text{A.8})$$

■

Lemma A.3 (Moment gradient operator II) *The moment gradient as defined by (A.4)–(A.7) applied to the function $f(\underline{\omega}, \underline{\mu}) = \mu_k$ for some $k = 1, 2, \dots, N$ is the following vector:*

$$\mathbb{R}^{2N} \ni \underline{b} := [b_0, b_1, \dots, b_{2N-1}]^T = \nabla_{\underline{M}} \mu_k = \underline{B}^{-1} \nabla_{(\underline{\omega}, \underline{\mu})} \mu_k = \underline{B}^{-1} \underline{e}_{N+k}, \quad (\text{A.9})$$

where $\underline{e}_{N+k} \in \mathbb{R}^{2N}$ is a vector with value of one in component $N+k$ and a value of zero in all other components.

Furthermore, \underline{b} as defined above can be interpreted as the vector of coefficients of the following polynomial:

$$Q_{2N-1}(v) := b_0 + b_1 v + b_2 v^2 + \cdots + b_{2N-1} v^{2N-1} = \sum_{k=0}^{2N-1} b_k v^k, \quad (\text{A.10})$$

which satisfies all of the following conditions:

$$Q_{2N-1}(\mu_p) = 0 \quad \text{and} \quad Q'_{2N-1}(\mu_p) = \frac{1}{\omega_k} \delta_p^k \quad \text{for } p = 1, 2, \dots, N. \quad (\text{A.11})$$

The polynomial Q_{2N-1} can be explicitly written as follows:

$$Q_{2N-1}(v) = \frac{(v - \mu_k)}{\omega_k} \left[\prod_{\substack{p=1 \\ p \neq k}}^N (v - \mu_p)^2 \right] \left/ \prod_{\substack{p=1 \\ p \neq k}}^N (\mu_k - \mu_p)^2 \right. \right]. \quad (\text{A.12})$$

Finally, the dot product between the vector $\underline{b} \in \mathbb{R}^{2N}$ defined by (A.9) and the following vector:

$$\underline{r}(s) := [1, s, s^2, \dots, s^{2N-1}]^T, \quad s \in \mathbb{R}, \quad (\text{A.13})$$

can be written as

$$\underline{b} \cdot \underline{r}(s) = Q_{2N-1}(s) = \frac{(s - \mu_k)}{\omega_k} \left[\prod_{\substack{p=1 \\ p \neq k}}^N (s - \mu_p)^2 \right] \left/ \prod_{\substack{p=1 \\ p \neq k}}^N (\mu_k - \mu_p)^2 \right. \right]. \quad (\text{A.14})$$

Proof Equation (A.9) follows directly from definitions (A.4)–(A.7). Polynomial (A.10) with Hermite interpolation conditions (A.11) follows from an argument similar to the one provided in Lemma (A.1). Equation (A.12) follows from invoking the Lagrange form of the interpolating polynomial that satisfies conditions (A.11).

Finally, dot product (A.14) follows from the simple observation that

$$\begin{aligned} Q_{2N-1}(sv) &= \sum_{k=0}^{2N-1} b_k s^k v^k = b_0 + (b_1 s) v + \cdots + (b_{2N-1} s^{2N-1}) v^{2N-1} \\ \Rightarrow Q_{2N-1}(s) &= \sum_{k=0}^{2N-1} b_k r_k(s) = \underline{b} \cdot \underline{r}(s), \end{aligned}$$

which when combined with (A.12) gives the desired result. ■

Acknowledgments

This research was partially funded by NSF Grants DMS–1620128 and DMS–2012699.

References

1. Abdelmalik, M., van Brummelen, E.: Moment closure approximations of the Boltzmann equation based on φ -divergences. *J. Stat. Phys.* **164**, 77–104 (2016)
2. Böhmer, N., Torrilhon, M.: Entropic quadrature for moment approximations of the Boltzmann-BGK equation. *J. Comput. Phys.* **401**(108992) (2020)
3. Broadwell, J.: Study of rarefied shear flow by the discrete velocity method. *J. Fluid Mech.* **19**, 401–414 (1964)
4. Broadwell, J.E.: Shock structure in a simple discrete velocity gas. *Phys. Fluids* **7**, 1243–1247 (1964)
5. Cai, Z., Fan, Y., Li, R.: Globally hyperbolic regularization of grad’s moment system in one dimensional space. *Comm. Math. Sci.* **11**, 547–571 (2013)
6. Cai, Z., Fan, Y., Li, R.: Globally hyperbolic regularization of grad’s moment system. *Comm. Pure Appl. Math.* **32**, 464–518 (2014)
7. Chalons, C., Fox, R., Massot, M.: A multi-Gaussian quadrature method of moments for gas-particle flows in a LES framework. In: *Proceedings of the Summer Program*, pp. 347–358. Center for Turbulence Research (2010)
8. Chalons, C., Kah, D., Massot, M.: Beyond pressureless gas dynamics: Quadrature-based velocity moment models. *Comm. Math. Sci.* **10**, 1241–1272 (2012)
9. Cheng, Y., Rossmanith, J.: A class of quadrature-based moment-closure methods with application to the Vlasov-Poisson-Fokker-Planck system in the high-field limit. *J. Comput. Appl. Math.* **262**, 384–398 (2014)
10. Cockburn, B., Shu, C.W.: The Runge–Kutta discontinuous Galerkin method for conservation laws V. *J. Comput. Physics* **141**(2), 199–224 (1998). DOI 10.1006/jcph.1998.5892. URL <http://www.sciencedirect.com/science/article/pii/S0021999198958922>
11. Desjardins, O., Fox, R., Villedieu, P.: A quadrature-based moment method for dilute fluid-particle flows. *J. Comput. Phys.* **227**, 2514–2539 (2008)
12. Dreyer, W.: Maximisation of the entropy in non-equilibrium. *J Phys A-Math* **20**, 6505–6517 (1987)
13. Felton, C., Harris, M., Logemann, C., Nelson, S., Pelakh, I., Rossmanith, J.: A positivity-preserving limiting strategy for locally-implicit Lax-Wendroff discontinuous Galerkin methods. <https://arxiv.org/abs/1806.06756> (2018)
14. Fox, R.: *Computational Models for Turbulent Flows*. Cambridge University Press (2003)
15. Fox, R.: A quadrature-based third-order moment method for dilute gas-particle flows. *J. Comput. Phys.* **227**, 6313 – 6350 (2008)
16. Fox, R.: Higher-order quadrature-based moment methods for kinetic equations. *J. Comput. Phys.* **228**, 7771–7791 (2009)

17. Fox, R., Laurent, F., Vié, A.: Conditional hyperbolic quadrature method of moments for kinetic equations. *J. Comput. Phys.* **365**, 269–293 (2018)
18. Gassner, G., Dumbser, M., Hindenlang, F., Munz, C.D.: Explicit one-step time discretizations for discontinuous Galerkin and finite volume schemes based on local predictors. *J. Comput. Physics* **230**, 4232–4247 (2011)
19. Grad, H.: On the kinetic theory of rarefied gases. *Comm. Pure Appl. Math.* **2**, 331–407 (1949)
20. Guthrey, P., Rossmanith, J.: The regionally-implicit discontinuous Galerkin method: Improving the stability of DG-FEM. *SIAM J. Num. Analysis* **57**, 1263–1288 (2019)
21. Johnson, E.R.: A high-order discontinuous Galerkin finite element method for a quadrature-based moment-closure model. Master’s thesis, Iowa State University (2017)
22. Junk, M.: Domain of definition of Levermore’s five-moment system. *J. Stat. Phys.* **93**, 1143–1167 (1998)
23. Kamermans, M.: Gaussian quadrature weights and abscissae. URL <https://pomax.github.io/bezierinfo/legendre-gauss.html>
24. Koellermeier, J., Torrilhon, M.: Numerical solution of hyperbolic moment models for the Boltzmann equation. *Eur. J. Mech. B/Fluids* **64**, 41–46 (2017)
25. von Kowalesky, S.: Zur Theorie der partialen Differentialgleichungen. *Journal für die reine und angewandte Mathematik* **80**, 1–32 (1875)
26. Lax, P., Wendroff, B.: Systems of conservation laws. *Comm. Pure Appl. Math.* **13**, 217–237 (1960)
27. LeVeque, R.: Wave propagation algorithms for multi-dimensional hyperbolic systems. *J. Comp. Phys.* **131**, 327–335 (1997)
28. Levermore, C.: Moment closure hierarchies for kinetic theories. *J. Stat. Phys.* **83**, 1021–1065 (1996)
29. Marchisio, D., Fox, R.: Solution of population balance equations using the direct quadrature method of moments. *J. Aerosol Science* **36**, 43–73 (2005)
30. Moe, S., Rossmanith, J., Seal, D.: A simple and effective high-order shock-capturing limiter for discontinuous Galerkin methods (2015). <https://arxiv.org/abs/1507.03024>
31. Moe, S., Rossmanith, J., Seal, D.: Positivity-preserving discontinuous Galerkin methods with Lax-Wendroff time discretizations. *J. Sci. Comput.* **71**, 44–70 (2017)
32. Müller, I., Ruggeri, T.: Extended thermodynamics. Springer (1993)
33. Patel, R., Desjardins, O., Fox, R.: Three-dimensional conditional hyperbolic quadrature method of moments. *J. Comput. Physics: X* **1**(100006) (2019)
34. Platkowski, T., Illner, R.: Discrete velocity models of the Boltzmann equation: a survey on the mathematical aspects of the theory. *SIAM Rev.* **30**(2), 213–255 (1988)
35. Qiu, J., Dumbser, M., Shu, C.W.: The discontinuous Galerkin method with Lax-Wendroff type time discretizations. *Comput. Methods Appl. Mech. Engr.* **194**, 4528–4543 (2005)
36. Reed, W., Hill, T.: Triangular mesh methods for the neutron transport equation. Tech. Rep. LA-UR-73-479, Los Alamos Scientific Laboratory (1973)
37. Rusanov, V.: Calculation of interaction of non-steady shock waves with obstacles. *J. Comp. Math. Phys. USSR* **1**, 267–279 (1961)
38. Schmüdgen, K.: The Moment Problem. Graduate Texts in Mathematics. Springer (2017)
39. Süli, E., Mayers, D.: An Introduction to Numerical Analysis. Cambridge University Press (2003)
40. Titarev, V., Toro, E.: ADER: arbitrary high order Godunov approach. *J. Sci. Comput.* **17**, 609–618 (2002)
41. Vikas, V., Wang, Z., Passalacqua, A., Fox, R.: Realizable high-order finite-volume schemes for quadrature-based moment methods. *J. Comp. Phys.* **230**, 5328 – 5352 (2011)
42. Wiersma, C.: A locally-implicit Lax-Wendroff discontinuous Galerkin scheme with limiters that guarantees moment-realizability for quadrature-based moment closures. Master’s thesis, Iowa State University (2019)
43. Zhang, X., Shu, C.W.: Maximum-principle-satisfying and positivity-preserving high-order schemes for conservation laws: Survey and new developments. *Proc. R. Soc. A* **467**, 2752–2776 (2011)
44. Zhang, X., Shu, C.W.: Positivity-preserving high order discontinuous Galerkin schemes for compressible Euler equations with source terms. *J. Comput. Phys.* **230**, 1238–1248 (2011)